

1 **Exploring prokaryotic transcription, operon structures, rRNA maturation**
2 **and modifications using Nanopore-based native RNA sequencing**

3

4 Felix Grünberger¹, Robert Knüppel², Michael Jüttner², Martin Fenk¹, Andreas Borst³, Robert Reichelt¹,
5 Winfried Hausner¹, Jörg Soppa³, Sébastien Ferreira-Cerca^{2*}, and Dina Grohmann^{1,4*}

6

7 ¹ Institute of Biochemistry, Genetics and Microbiology, Institute of Microbiology and Archaea Centre,
8 Single-Molecule Biochemistry Lab, University of Regensburg, Universitätsstraße 31, 93053 Regensburg,
9 Germany

10 ² Institute for Biochemistry, Genetics and Microbiology, Biochemistry III, University of Regensburg,
11 Universitätsstraße, 31, 93053 Regensburg, Germany

12 ³ Goethe-University, Biocentre, Institute for Molecular Biosciences, Max-von-Laue-Str. 9, 60439
13 Frankfurt, Germany

14 ⁴ Regensburg Center of Biochemistry (RCB), University of Regensburg, 93053 Regensburg, Germany

15

16

17 *For correspondence:

18 Sébastien Ferreira-Cerca
19 Biochemistry III – Institute for Biochemistry, Genetics and Microbiology, University of Regensburg,
20 Universitätsstraße 31, 93053 Regensburg, Germany.

21 e-mail: sebastien.ferreira-cerca@ur.de

22 Tel.: 0049 941 943 2539

23 Fax: 0049 941 943 2474

24

25 Dina Grohmann
26 Department of Biochemistry, Genetics and Microbiology, Institute of Microbiology, University of
27 Regensburg, Universitätsstraße 31, 93053 Regensburg, Germany

28 e-mail: dina.grohmann@ur.de

29 Tel.: 0049 941 943 3147

30 Fax: 0049 941 943 2403

31

32 **Keywords:** Nanopore, RNA-seq, next generation sequencing, transcription, ribosomal RNA, RNA
33 modifications, transcriptome, archaea, bacteria

34 **Abstract**

35 The prokaryotic transcriptome is shaped by transcriptional and posttranscriptional events that
36 define the characteristics of an RNA, including transcript boundaries, the base modification status,
37 and processing pathways to yield mature RNAs. Currently, a combination of several specialised
38 short-read sequencing approaches and additional biochemical experiments are required to
39 describe all transcriptomic features. In this study, we present native RNA sequencing of bacterial
40 (*E. coli*) and archaeal (*H. volcanii*, *P. furiosus*) transcriptomes employing the Oxford Nanopore
41 sequencing technology. Based on this approach, we could address multiple transcriptomic
42 characteristics simultaneously with single-molecule resolution. Taking advantage of long RNA
43 reads provided by the Nanopore platform, we could (re-)annotate large transcriptional units and
44 boundaries. Our analysis of transcription termination sites suggests that diverse termination
45 mechanisms are in place in archaea. Moreover, we shed additional light on the poorly understood
46 rRNA processing pathway in Archaea. One of the key features of native RNA sequencing is that RNA
47 modifications are retained. We could confirm this ability by analysing the well-known KsgA-
48 dependent methylation sites and mapping of N⁴-acetylcytosines modifications in rRNAs. Notably,
49 we were able to follow the relative timely order of the installation of these modifications in the
50 rRNA processing pathway.

51

52

53

54 Introduction

55 In the last decade, next-generation sequencing (NGS) technologies¹ revolutionized the field of
56 microbiology², which is not only reflected in the exponential increase in the number of fully
57 sequenced microbial genomes, but also in the detection of microbial diversity in many hitherto
58 inaccessible habitats based on metagenomics. Using transcriptomics, important advances were
59 also possible in the field of RNA biology^{3,4} that shaped our understanding of the transcriptional
60 landscape^{5,6} and RNA-mediated regulatory processes in prokaryotes⁷. RNA sequencing (RNA-seq)
61 technologies can be categorized according to their platform-dependent read lengths and necessity
62 of a reverse transcription and amplification step to generate cDNA⁸. Illumina sequencing yields
63 highly accurate yet short sequencing reads (commonly 100-300 bp). Hence, sequence information
64 is only available in a fragmented form, making full-length transcript- or isoform-detection a
65 challenging task^{9,10}. Sequencing platforms developed by Pacific Bioscience (PacBio) and Oxford
66 Nanopore Technologies (ONT) solved this issue. Both sequencing methods are *bona fide* single-
67 molecule sequencing techniques that allow sequencing of long DNAs or RNAs^{11,12}. However, the
68 base detection differs significantly between the two methods. PacBio-sequencers rely on
69 fluorescence-based single-molecule detection that identifies bases based on the unique fluorescent
70 signal of each nucleotide during DNA synthesis by a dedicated polymerase¹². In contrast, in an ONT
71 sequencer, the DNA or RNA molecule is pushed through a membrane-bound biological pore with
72 the aid of a motor protein that is attached to the pore protein called a nanopore (Fig. 1a). A change
73 in current is caused by the translocation of the DNA or RNA strand through this nanopore, which
74 serves as a readout signal for the sequencing process. Due to the length of the nanopore (version
75 R9.4), a stretch of approximately five bases contributes to the current signal. Notably, only ONT
76 offers the possibility to directly sequence native RNAs without the need for prior cDNA synthesis
77 and PCR amplification¹³. Direct RNA sequencing based on the PacBio platform has also been
78 realised but requires a customised sequencing workflow using a reverse transcriptase in the
79 sequencing hotspot instead of a standard DNA polymerase¹⁴. Native RNA-seq holds the capacity to
80 sequence full-length transcripts and first attempts have been made to use ONT sequencing to
81 identify RNA base modifications (e.g. methylations^{15,16}). ONT sequencing is a *bona fide* single-
82 molecule technique and hence offers the possibility to detect molecular heterogeneity in a

83 transcriptome¹⁷. Recently, the technology was exploited to sequence viral RNA genomes¹⁸⁻²² to
84 gain insights into viral and eukaryotic transcriptomes^{18,23-25} and to detect RNA isoforms in
85 eukaryotes^{26,27}. However, prokaryotic transcriptomes have not been characterized on the genome-
86 wide level by native RNA-seq approaches so far as prokaryotic RNAs lack a poly(A) tail, which is
87 required to capture the RNA and feed it into the nanopore.

88 Here, we present a native RNA sequencing study of bacterial and archaeal transcriptomes using
89 Nanopore technology. We employed an experimental workflow that includes the enzymatic
90 polyadenylation of prokaryotic transcriptomes to make them amenable for ONT's direct RNA
91 sequencing kit. In the first part, we evaluated the applicability of the ONT native RNA sequencing
92 approach to survey transcriptomic features in prokaryotes and discuss weaknesses and strengths
93 of this method. To this end, we assessed the accuracy and reliability of native RNA-seq in
94 comparison to published Illumina-based sequencing studies of bacterial (*Escherichia coli*) and
95 archaeal (*Haloferax volcanii*, *Pyrococcus furiosus*) model organisms²⁸⁻³³. The transcriptomic
96 analysis included determination of transcript boundaries, providing, among others, insights into
97 termination mechanisms in archaea. We moreover tested the applicability of the ONT-based native
98 RNA sequencing approach i) to identify transcription units, (ii) to analyze pre-ribosomal RNA
99 processing pathways and iii) to identify base modifications in (pre-)rRNAs. Despite, intrinsic
100 limitations of the ONT-platform, we demonstrate that the long RNA reads gathered on the ONT
101 platform allow reliable transcriptional unit assignment. Strikingly, we gained insights into the so
102 far poorly understood ribosomal RNA (rRNA) maturation pathway in Archaea. As RNA
103 modifications are retained when sequencing native RNAs, we explored the possibility to trace a
104 selection of rRNA modifications in prokaryotes. Moreover, we provide data that position the
105 relative timely order of the KsgA-dependent methylation and acetylation of rRNAs in archaea.
106 Together, our comparative analysis suggests that rRNA modifications are more abundant in an
107 hyperthermophilic organism.

108

109

110 **Material and Methods**

111 **Strains and growth conditions**

112 *Escherichia coli* K-12 MG1655 cells were grown in LB medium (10 g tryptone, 5 g yeast extract, 10
113 g NaCl per liter) to an OD_{600nm} of 0.5 and harvested by centrifugation at 3,939 x g for 10 min at 4°C.

114

115 *Pyrococcus furiosus* strain DSM 3638 cells were grown anaerobically in 40 ml SME medium³⁴
116 supplemented with 40 mM pyruvate, 0.1 % peptone and 0.1 % yeast extract at 95°C to mid-
117 exponential phase and further harvested by centrifugation at 3,939 x g for 45 min at 4°C.

118

119 Markerless deletion of *Haloferax volcanii* KsgA (Hvo_2746) was obtained using the pop-in/pop-out
120 procedure³⁵. Deletion candidates were verified by Southern blot and PCR analyses. Full
121 characterization of this strain will be described elsewhere (Knüppel and Ferreira-Cerca, *in*
122 *preparation*). Wildtype (H26) and Δ ksgA strains were grown in Hv-YPC medium at 42°C under
123 agitation as described previously³⁶.

124

125 **RNA isolation**

126 *E. coli* total RNA was purified using the Monarch® Total RNA Miniprep Kit (New England Biolabs)
127 according to manufacturer's instructions including the recommended on-column DNase
128 treatment.

129 *P. furiosus* total RNA was purified as described previously³³. In short, cell pellets were lysed by the
130 addition of 1 ml peqGOLD TriFast™ (VWR) followed by shaking for 10 min at room temperature.
131 After adding 0.2 ml 2 M sodium acetate pH 4.0, total RNA was isolated according to the
132 manufacturer's instructions. Contaminating DNA was removed using the TURBO DNA-free™ Kit
133 (Thermo Fisher Scientific).

134 *H. volcanii* total RNA was purified using the RNeasy kit (Qiagen) according to the manufacturer's
135 instructions. Alternatively, total RNA was isolated according to the method described by
136 Chomczynski and Sacchi³⁷, including a DNA-removal step with RNase-free DNase I (Thermo Fisher
137 Scientific).

138

139 The integrity of total RNA from *E. coli* and *P. furiosus* was assessed via a Bioanalyzer (Agilent) run
140 using the RNA 6000 Pico Kit (Agilent). To evaluate the extent of remaining buffer and DNA
141 contaminations, the RNA preparation samples were tested by performing standard spectroscopic
142 measurements (Nanodrop One) and using the Qubit 1X dsDNA HS assay kit (Thermo Fisher
143 Scientific). RNA was quantified using the Qubit RNA HS assay kit.

144

145 **Primer extension analysis**

146 5'ends determination of mature 16S and 23S rRNAs from *H. volcanii* by primer extension was
147 performed as described previously (Knüppel et al, Method in Molecular Biology *in press*). In brief,
148 reverse transcription was performed with the indicated fluorescently labeled primers (oHv396-
149 DY682: 5'-CCCAATAGCAATGACCTCCG; oHv622-DY782: 5'-GCTCTCGAGCCGAGCTATCCACC) and
150 SuperScript III reverse transcriptase using 1 µg of total RNA as template. The resulting cDNAs and
151 reference dideoxy-chain termination sequencing ladder reactions were separated on a denaturing
152 14% TBE-Urea (6 M)-PAGE. Fluorescence signals (700nm and 800nm) were acquired using a Li-
153 COR Odyssey system.

154

155 ***In vitro* transcription assays**

156 RNA polymerase from *P. furiosus* cells and recombinant TBP and TFB were purified as described
157 previously³⁸⁻⁴⁰. The gene encoding histone A1 (*hpyA1*) as well as the native promoter and
158 terminator regions was used as template for transcription reactions as described in⁴¹.
159 Run-off transcription assays^{42,43} were carried out in a 25-µl reaction volume containing the
160 following buffer: 40 mM HEPES (pH 7.5), 2.5 mM MgCl₂, 0.125 mM EDTA, 0.25 M KCl, 20 µg/ml
161 BSA supplied with 100 µM ATP, 100 µM GTP, 100 µM CTP, 2 µM UTP, 0.037 MBq [α -³²P]-UTP
162 (Hartmann Analytics) with 8.5 nM *hpy1A* template DNA, 10.5 nM RNAP, 85 nM TBP and 52 nM TFB.
163 Reactions were incubated at 80°C or 90°C for 10 min. The radiolabeled products were extracted
164 with phenol/chloroform and transcription products were separated on a 8%TBE-Urea (7M)-PAGE.
165 The gel was transferred and fixed to a Whatman chromatography paper.

166 Gels with radioactive samples were exposed to an Imaging Plate for autoradiography. Signals
167 derived from radiolabeled RNA transcripts were detected with FUJIFILM FLA 7000
168 PhosphorImager (Fuji) and analysed with Image Lab™ Software (Biorad).

169

170 **RNA treatment and poly(A)-tailing**

171 To prevent secondary structure formation, the RNA was heat incubated at 70°C for 3 min and
172 immediately put on ice before TEX-treatment or poly(A)-tailing of the RNA samples. Partial
173 digestion of RNAs that are not 5'-triphosphorylated (e.g. tRNAs, rRNAs) was achieved by
174 incubation of the RNA with the Terminator 5'-Phosphate-Dependent Exonuclease (TEX, Lucigen).
175 For this purpose, 10 µg of RNA were incubated with 1 unit TEX, 2 µl TEX reaction buffer (Lucigen)
176 and 0.5 µl RiboGuard RNase Inhibitor (Lucigen) in a total volume of 20 µl for 60 minutes at 30°C.
177 The reaction was stopped and the RNA was purified using the RNeasy MinElute Cleanup Kit
178 (Qiagen). For *P. furiosus* and *E. coli* RNA samples, control reactions lacking the exonuclease
179 (NOTEX) were treated as described for TEX-containing samples. In the next step, a poly(A)-tail was
180 added using the *E. coli* poly(A) polymerase (New England Biolabs) following a recently published
181 protocol⁴⁴. Briefly, 5 µg RNA, 20 units poly(A) polymerase, 2 µl reaction buffer and 1 mM ATP were
182 incubated for 15 min at 37°C in a total reaction volume of 50 µl. To stop the reaction and to remove
183 the enzyme, the poly(A)-tailed RNA was purified with the RNeasy MinElute Cleanup Kit (Qiagen).

184

185 **Direct RNA library preparation and sequencing**

186 Libraries for Nanopore sequencing were prepared from poly(A)-tailed RNAs according to the SQK-
187 RNA001 Kit protocol (Oxford Nanopore, Version: DRS_9026_v1_revP_15Dec2016) with minor
188 modifications for barcoded libraries (see Supplementary Fig. 1a). In this case, Agencourt AMPure
189 XP magnetic beads (Beckman Coulter) in combination with 1 µl of RiboGuard RNase Inhibitor
190 (Lucigen) were used instead of the recommended Agencourt RNAClean XP beads to purify samples
191 after enzymatic reactions. The total amount of input RNA, the barcoding strategy and the number
192 of flowcells used can be found in Supplementary Table 1. The efficiency of poly(A)-tailing was low.
193 However, this could be compensated with a higher amount of input RNA. We added the control

194 RNA (RCS, yeast enolase, provided in the SQK-RNA001 kit) to detect problems that arise from
195 library preparation or sequencing. For the barcoded libraries, the RTA adapter was replaced by
196 custom adapters described in <https://github.com/hyeshik/poreplex> and reverse transcription
197 (RT) was performed in individual tubes for each library. After RT reactions, cDNA was quantified
198 using the Qubit DNA HS assay kit (Thermo Fisher Scientific) and equimolar amounts of DNA for
199 the multiplexed samples were used in the next step for ligation of the RNA Adapter (RMX) in a
200 single tube. Subsequent reactions were performed according to the protocols recommended by
201 ONT. The libraries were sequenced on a MinION using R9.4 flow cells and subsequently, FAST5
202 files were generated using the recommended script in MinKNOW.

203

204 **Data analysis**

205 *Demultiplexing of raw reads, basecalling and quality control of raw reads*

206 As some bioinformatic tools depend on single-read files we first converted multi-read FAST5 files
207 from the MinKNOW output to single-read FAST5 files using the `ont_fast5_api` from Oxford
208 Nanopore (https://github.com/nanoporetech/ont_fast5_api). To prevent actual good-quality
209 reads from being discarded (this issue was reported previously^{13,45}), we included both failed and
210 passed read folders in the following steps of the analysis. Demultiplexing was done by `poreplex`
211 (version 0.4, <https://github.com/hyeshik/poreplex>) with the arguments `--trim-adapter`, `--`
212 `symlink-fast5`, `--basecall` and `--barcoding`, to trim off adapter sequences in output FASTQ files,
213 basecall using `albacore`, create symbolic links to FAST5 files and sort the reads according to their
214 barcodes. However, to ensure consistency between non-multiplexed and multiplexed samples and
215 because of some major improvements in the current basecalling software (`guppy`), `albacore` files
216 were not used. Instead demultiplexed FAST5 reads and raw FAST5 reads from non-multiplexed
217 runs were locally basecalled using `Guppy` (Version 3.0.3) with `--reverse_sequence`, `--hp_correct`, `--`
218 `enable_trimming` and `--calib_detect` turned on. After that, relevant information from the
219 `sequencing_summary.txt` file in the `Guppy` output was extracted to analyse properties of raw reads
220 (see Supplementary Fig. 2, see Supplementary Table 1).

221

222 *Mapping of reads and quantification*

223 Files were mapped to reference genomes from *Escherichia coli* K12 MG1655 (GenBank:
224 U00096.2)⁴⁶, *Haloferax volcanii* (NCBI Reference Sequence NC_013967)⁴⁷ and *Pyrococcus furiosus*
225 DSM3638³³ using minimap2 (Release 2.17-r941, <https://github.com/lh3/minimap2>)⁴⁸. Output
226 alignments in the SAM format were generated with the recommended options for noisy Nanopore
227 Direct RNA-seq (-ax splice, -uf, -k14) and also with (1) -p set to 0.99, to return primary and
228 secondary mappings and (2) with --MD turned on, to include the MD tag for calculating mapping
229 identities. Alignment files were further converted to bam files, sorted and indexed using
230 SAMtools⁴⁹. Strand-specific wig and bigwig files were finally created using bam2wig (Version 1.5,
231 <https://github.com/MikeAxtell/bam2wig>). To evaluate the alignments, we first calculated the
232 aligned read length by adding the number of M and I characters in the CIGAR string¹³. Based on
233 this, the mapping identity was defined as $(1 - \text{NM} / \text{aligned_reads}) * 100$, where NM is the edit
234 distance reported taken from minimap2. Read basecalling and mapping metrics can be found in
235 Supplementary Table 1. Transcriptome coverage was estimated by dividing the total number of
236 CDS-mapping reads by the sum of all CDS genomic regions.

237

238 *Gene expression analysis*

239 For transcript abundance estimation we applied featureCounts (Rsubread 1.32.4) allowing that a
240 read can be assigned to more than one feature (allowMultiOverlap = TRUE) and applying the
241 setting for long reads (isLongRead = TRUE)⁵⁰. Calculations were performed based on the genome
242 coordinates of genomic feature types (tRNA, rRNA, protein-coding genes). For the abundance
243 comparison to Illumina-sequencing, we applied a regularized log transformation from the DESeq2
244 package that transforms counts to a log₂ scale, normalizing for the library size and minimizing
245 differences between samples with small counts⁵¹ (raw count data for TEX samples in
246 Supplementary Table 2).

247

248 *Poly(A) tail analysis*

249 Poly(A) tail length was estimated by nanopolish following the recommended workflow (Version
250 0.10.2, https://nanopolish.readthedocs.io/en/latest/quickstart_polya.html)⁵².

251

252 *Detection of transcriptional units and annotation of transcription start sites and transcription*
253 *termination sites*

254 The definition of transcriptional units (TU) and our strategy to detect and annotate them was
255 based on a recent study that re-defined the bioinformatical search for transcriptional units (TU)³¹.

256 The TU annotation was performed in a two-step process in the following way: First, TU clusters
257 were defined by collapsing all reads that overlap and fulfill certain criteria that are commented

258 extensively in the available code for this study
259 (https://github.com/felixgrunberger/Native_RNAseq_Microbes). In short, reads were filtered out

260 that did not align protein-coding genes (CDS) or tRNAs, had a mapping identity below 80%, were
261 spliced, were shorter than 50% of the gene body and did not cover either the 5' or the 3'

262 untranslated region. The remaining overlapping reads were collapsed in a strand-specific manner
263 and merged.

264 Finally, the collapsed reads that represent the TU cluster, were split according to the coverage drop
265 at the 3' region of a gene. This was achieved by calculating the sequencing depth in a window of

266 20 nt upstream and downstream of the corresponding TTS and applying a deliberately low
267 threshold of 1.5x (higher coverage upstream compared to downstream, see transcriptional unit

268 table in Supplementary Table 5).

269 TSS were predicted by calculating the median start position of all reads that map to one gene and
270 cover the 5' part of a CDS. To address the 3' coverage bias and the underrepresentation of reads

271 that map to the 5' end and also for the 12 missing nucleotides at the TSS in general, all reads starting
272 at least 20 nt downstream of the annotated gene start were included. To not exclude too many

273 reads, the position of TTS were predicted similarly, by also including reads that have end positions
274 starting from 20 nt upstream of a gene end (TSS table in Supplementary Table 3, TTS table in

275 Supplementary Table 4).

276 For the analysis of prokaryotic promoter elements, the sequences 46 basepairs upstream of the
277 corrected transcription start site were analysed to identify relevant motifs using MEME with

278 default options except for a custom background file, calculated from intergenic sequences of the
279 respective organism⁵³.

280 The analysis of terminator sequences was performed comparably by extracting all TTS that are
281 located at the end of a TU and searching for terminators in a sequence window from -45

282 (upstream) to +45 (downstream) from the TTS using MEME and the custom background model.
283 Heatmap analysis of motif positioning was performed by importing MEME FASTA information into
284 R. Metaplots of the nucleotide enrichment analysis (compare^{28,54}) were calculated by comparing
285 the genomic sequences surrounding a TTS in a window from -45 to 45 to randomly selected
286 intergenic positions (subsampling, n = 10000). Next, the log₂-fold enrichment was calculated and
287 plotted as in Fig. 2e and Supplementary Fig. 7b.

288 RNA structural stability was predicted by folding the 45 nt long DNA upstream of the TTS using
289 the RNAfold software from the Vienna RNA package⁵⁵. The results were compared to randomly
290 selected intergenic positions of the respective organism (size = 45 nt, n = 10000) and to published
291 TTS positions derived from Term-Seq data^{54,56}.

292 Additionally, accuracy of TTS prediction was analysed by comparing the 3'UTRs in *H. volcanii* for
293 genes, that were detected in both Term-Seq and Nanopore data (TEX set *H. volcanii* was used for
294 this analysis⁵⁶). The strength of the association between the two variables was investigated by
295 calculating Pearson's correlation coefficient.

296

297 *Detection of rRNA processing sites and classification of rRNA intermediates*

298 Processing site detection in bacteria and archaea was done by enrichment analysis of start and end
299 positions of reads mapping to the relevant rRNA region. Next, co-occurrence analysis in *E. coli* was
300 performed by (i) categorizing reads according to enriched and literature-expected 5' positions, (ii)
301 selecting all reads that start within +/-1 from the relevant 5' position and (iii) analysing the
302 respective read ends. Note that non-circular reads were 5'-extended by 12 nucleotides which
303 corresponds to the actual transcript start. Exemplary reads of selected categories with enriched
304 connected terminal positions were visualised in a genome browser-like view.

305 In addition to terminal enriched positions, read categories in archaea are based on the number of
306 junctions that are detected (njunc argument, compare post-16S-bhb/pre-ligation and RNA
307 chimera category in Supplementary Fig. 14), and clipping properties of the alignments on the 5'
308 end of the reads (see circular RNA detection).

309

310 *Circular RNA detection and confirmation*

311 Circular reads were initially observed in a subset of reads, which end near/at the 5' cleavage site
312 of the bulge-helix-bulge (bhb), but are extensively left-clipped, which happens during mapping if
313 the nucleotides further upstream do not match the 5' leading, but the 3' trailing region of the rRNA.
314 Accuracy of 5' and 3' cleavage site detection using Nanopore reads was further evaluated by
315 secondary structure prediction of the potential bulge-helix-bulge regions using RNAfold⁵⁵.
316 To investigate circular rRNA reads in more detail, a permuted linear sequence was created. This
317 sequence contained 500 nt upstream of the annotated rRNA end to the predicted 3' cleavage site
318 of the bhb site and was joined with the 5' cleavage site of the bhb up to 500 nt downstream of the
319 annotated rRNA start. Nanopore reads were re-mapped to the linear permuted sequence and again
320 categorised by their 5' ends and 3' ends as circular (3' random breaks within the rRNA) or opened-
321 circular (3' breaks at mature rRNA start, compare Supplementary Fig. 15). Additionally, a shorter
322 permuted sequence was created that included x-1 nt upstream and downstream of 3'-bhb cleavage
323 and 5'-bhb cleavage, respectively, where x is depending on the available read length of the
324 additional Illumina data sets used (*H. volcanii*: 100 nt, ; *P. furiosus*: 75 nt)^{29,33}. Illumina reads were
325 also re-mapped to the permuted sequence using bowtie2, allowing for no mismatches (-D1 -N 0 -
326 L32 -I S,1,0.50 --score-min C,0,0) and filtering out all reads that do not overlap the joined 3'-to-5'-
327 bulge.

328

329 *Modified base detection*

330 The performance of two different approaches (Tombo vs. basecalling properties) for the detection
331 of modified bases was evaluated:

332 (1) We used Tombo (Version 1.5.1, <https://nanoporetech.github.io/tombo>) to identify modified
333 bases based on a comparison to a theoretical distribution (*de novo* model) and based on the
334 comparison to a reference data set (sample-compare model)⁵⁷. Briefly, for Fig. 6f reads mapping
335 to 16S rRNA were preprocessed, resquiggled and the raw signal plotted at a specific genomic
336 coordinate using the respective plotting command (tombo plot genome_locations). In addition, the
337 probability of modified bases was calculated using the detect_modification de_novo command. For
338 Fig. 6g the signals were calculated for both samples (wildtype and deletion mutant) and compared
339 using the *control-fast5-basedirs* and *overplot Boxplot* option. For Fig 7b reference data sets were
340 created by sorting the reads mapping to the 16S rRNA based on the pre-determined rRNA

341 maturation categories. 5'-extended pre-rRNA were used in all cases as a background data set in
342 the sample-compare approach. Probabilities were calculated for the sample-compare model for all
343 read categories and plotted using custom R-scripts.

344 (2) For calculating the frequency of correct, deleted, inserted and wrong nucleotides at a genomic
345 position *pysamstats* (<https://github.com/alimanfoo/pysamstats>) was used. Plots were generated
346 using custom R scripts. The results were compared to known modification sites in 16S rRNA for *H.*
347 *volcanii*⁵⁸ and *P. furiosus*. Note that the positions of modified RNA base modifications for *P. furiosus*
348 are derived from a recently published study in *P. abyssi*⁵⁹.

349

350 **Public data**

351 In addition to the in-house generated data, we made use of other published sequencing data sets
352 and data repositories that are described in the following.

353

354 *Transcriptional start sites*

355 For all three model organisms, global transcriptional start sites were mapped recently using
356 differential RNA sequencing^{29,32,33}. Position data were extracted from the Supplementary data of
357 the publications and compared with the TSS described in the ONT data sets given that a start site
358 was found in both data sets.

359

360 *Transcriptional termination sites*

361 So far there is no transcription termination data set available for *P. furiosus*. The 3' UTR lengths of
362 the *E. coli* and *H. volcanii* ONT sets were compared to TTS predicted based on the Term-Seq
363 method^{28,56}.

364

365 *Transcriptional units*

366 The widely used database DOOR2⁶⁰ was used to compare the TU annotation for both archaeal sets.
367 For *E. coli* a more recent, but also purely bioinformatical prediction, served as a reference set³¹.

368

369 *Gene expression comparison*

370 For *P. furiosus* gene abundances from ONT data were compared to fragmented RNA sequencing
371 data of mixed growth conditions (conditions, library, sequencing, mapping described in³³), by
372 applying a regularized log transformation as described earlier⁵¹. For *H. volcanii* comparison, raw
373 reads of a mixed RNA sequencing were extracted from the Sequence Read Archive SRA
374 (SRR7811297)³⁰ trimmed using trimmomatic⁶¹, (leading:20, trailing:20, slidingwindow:4:20,
375 minlen:12), mapped to the reference genome using bowtie2 (-N 0, -L 26)⁶², converted to sorted
376 bam files using samtools⁴⁹ and compared to ONT data as described for *P. furiosus*. Illumina RNA
377 sequencing data for *E. coli* were also extracted from the NCBI (SRP056485, 37°C LB), analysed as
378 described for *H. volcanii* Illumina data and also compared to the ONT reference data.

379

380 *Confirmation of circular rRNA precursors*

381 For the confirmation of circular rRNA precursors we re-mapped Illumina reads to permuted rRNA
382 sequences (see above). Illumina RNA sequencing data for *H. volcanii* (SRR3623113)²⁹ and *P.*
383 *furiosus* (SRR8767848)³³ were obtained from the SRA.

384

385 **Results**

386 **Library preparation for Nanopore native RNA sequencing of bacterial and archaeal transcriptomes**

387 ONT allows single-molecule sequencing of RNAs in their native form. However, at present, the
388 direct RNA sequencing kit is designed to capture polyadenylated transcripts in the first step of
389 library preparation. As prokaryotic RNAs are not polyadenylated, we first set up a workflow that
390 allows whole-transcriptome native RNA sequencing using the Nanopore sequencing technology
391 (referred to as Nanopore native RNA sequencing in this work) and that can be applied to any
392 prokaryotic organism. The key steps of the library preparation are shown in Fig. 1a: after
393 enzymatic polyadenylation, the RNA is reverse transcribed to improve the performance by
394 resolving secondary structures at the 3' end (recommended by ONT)¹⁷. Please note that, despite
395 the synthesis of a cDNA strand during the reverse transcription step, the RNA strand and not the
396 DNA strand is fed into the Nanopore by the motor protein. Following this workflow, native RNAs
397 from prokaryotic organisms can be sequenced. Depending on the necessary sequencing depth, the
398 libraries were barcoded using poreplex (<https://github.com/hyeshik/poreplex>), since this is not
399 yet supported by the official kits and protocols from Oxford Nanopore. To discriminate primary
400 from mature rRNAs, we used a terminator exonuclease (TEX) specifically targeting 5'-
401 monophosphorylated ends of transcripts and compared them to non-treated samples (NOTEX, see
402 Supplementary Fig. 1a). The trimming effect of the exonuclease leads to the degradation of mature
403 rRNAs and in turn to an enrichment of terminal positions in the non-treated samples, ultimately
404 allowing the annotation of rRNA transcription start sites and mature rRNAs. In contrast to the
405 experimental design of a differential RNA-seq approach, where TEX is used to detect primary
406 transcripts in preferentially rRNA-depleted samples, we did not expect to see an effect on mRNAs,
407 given the overall excess of rRNAs. In addition, as many Illumina sequencing-based approaches
408 make use of a specialised library preparation design to tackle a well-defined question⁸, we
409 evaluated the potential of native RNA sequencing to analyse multiple transcriptomic features
410 simultaneously including the identification of *cis*-regulatory elements that govern transcription,
411 the analysis of operon structures and transcriptional boundaries, rRNA processing and rRNA
412 modification patterns (see Supplementary Fig. 1b).

413

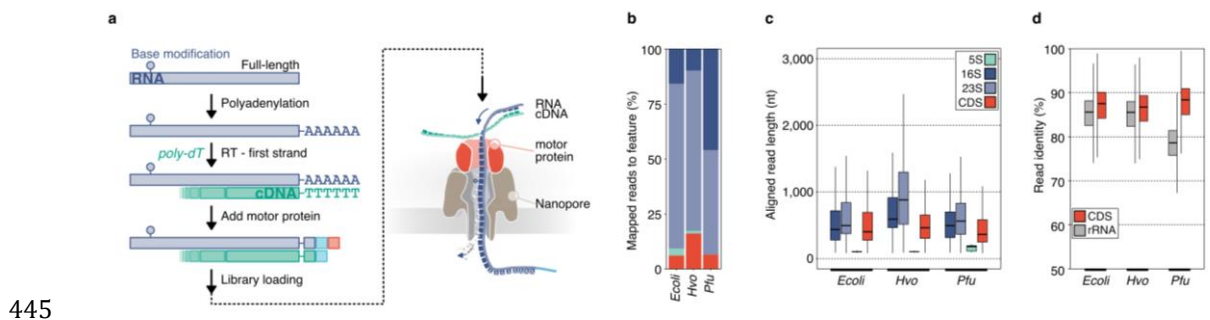
414 **Sequencing yield and quality control of raw Nanopore reads**

415 Native RNA sequencing was performed for three prokaryotic organisms: the bacterial model
416 organism *Escherichia coli*, the halophilic archaeon *Haloferax volcanii* and the hyperthermophilic
417 archaeon *Pyrococcus furiosus*. In order to show that native RNA sequencing can be applied to a
418 wide variety of prokaryotic organisms, we specifically chose (i) organisms from the bacterial and
419 archaeal domain of life with *P. furiosus* and *H. volcanii* belonging to the Euryarchaeota, (ii)
420 organisms that are classified as mesophilic (*E. coli*, *H. volcanii*), hyperthermophilic (*P. furiosus*), or
421 halophilic organism (*H. volcanii*) and (iii) organisms that differ significantly in their GC-content (*E.*
422 *coli*: 50.8%⁶³, *H. volcanii*: 65%⁴⁷, *P. furiosus*: 40.8%³³). The prepared libraries were sequenced on a
423 MinION device and reads were collected over 48 hours on R9.4 flow cells (see Supplementary Fig.
424 2a). Although we did not deplete rRNAs, the total number of reads was still sufficient to also
425 achieve good coverage of the mRNA transcriptome (*E. coli*: 9.2x, *P. furiosus*: 15.0x, *H. volcanii*: 10.3x,
426 see Supplementary Table 1), which allowed us to perform transcriptional unit annotation and
427 determination of transcript boundaries. Before mapping the reads to the reference genomes, the
428 quality of the sequencing runs were evaluated based on raw read length distribution and quality
429 of reads estimated by Guppy (see Supplementary Fig. 2b,c). To verify that no problems occurred
430 during sequencing or library preparation the poly-adenylated spike-in control (yeast enolase)
431 provided in the ONT-RNA kit was used. The control showed a uniform length distribution (median
432 lengths between 1212 and 1306 nucleotides) and a very good read quality (median quality as
433 ascertained by the Phred score between 10.8 and 12.2) in all samples, therefore, excluding any bias
434 during sequencing (see Supplementary Fig. 2b,c, Supplementary Table 1). Lower quality in the
435 original samples as compared to the spike-in control can be attributed to multiple reasons,
436 including (i) compositional differences to the RNAs used to train the basecaller, and (ii) the fact
437 that mostly ribosomal RNAs are sequenced in our samples that are known to harbor base
438 modifications, which in turn may lead to a lower quality score especially in *P. furiosus*⁶⁴.

439 **Analysis of mapped reads**

440 An advantage of the long-read Nanopore sequencing technique is that native RNA strands can be
441 sequenced directly as near full-length transcripts⁶⁵. This is also reflected in the sequenced data
442 sets as aligned lengths up to 7864 nt can be observed (Fig. 1c, Supplementary Fig. 3c). As expected,

443 the majority of reads from all samples mapped to ribosomal RNAs, whereby the 23S rRNA
444 represents the largest proportion (Fig. 1b, see Supplementary Fig. 3a).



446 **Figure 1 | Nanopore-based native RNA sequencing of prokaryotes.** **a**, Key steps of library preparation: (1)
447 native RNA is polyadenylated, which allows library preparation using the direct RNA kit from Oxford
448 Nanopore and sequencing on a MinION device. (2) 3' ligation is performed to add an adapter carrying the
449 motor-protein (red square), which unzips the RNA-cDNA hybrid and pulls the RNA through the
450 Nanopore (detailed description see Supplementary Fig. 1a). **b**, Data sets for three prokaryotic model
451 organisms (*E. coli*: *Escherichia coli*, *Pfu*: *Pyrococcus furiosus*, *Hvo*: *Haloferax volcanii*) were collected and
452 mapped to their respective reference genome. Transcript abundances of genomic features (protein
453 coding genes (CDS): red, 5S rRNA: green, 16S rRNA: purple, 23S rRNA: light-purple) were estimated using
454 featurecounts⁵⁰ (TEX-treated samples are shown as example in Fig. 1). **c**, Aligned read lengths across
455 different genomic features. **d**, Comparison of read identities between CDS (red) and rRNA (grey)-
456 mapping reads.

457 In general, the read identity of CDS-mapping reads is higher than for rRNA mapping reads, but
458 lower than the spike-in control (Fig. 1d, see Supplementary Fig. 3b,c). It is noteworthy, that
459 accurate mapping of very short reads is currently not supported by the minimap2 mapping tool,
460 which explains the 100 nt cut-off in our data sets (see Supplementary Fig. 3d)^{17,48,66}. Unaligned
461 reads had a median read length of 191 nt, in contrast to 572 nt for aligned reads (all data sets
462 combined) suggesting that short reads could not be aligned properly. As small RNAs, CRISPR-RNAs
463 or tRNAs fall below this threshold, we excluded these RNAs from further analysis. While short
464 transcripts are problematic, longer RNAs can be sequenced and mapped accurately without loss in
465 quality (see Supplementary Fig. 3e). As the raw read quality correlates with the mapping identity
466 of the reads, problems during sequencing can be live-monitored in MinKNOW and the run can be
467 canceled allowing the loading of a new library (see Supplementary Fig. 3f). Since the subsequent
468 analysis of transcriptional units is heavily dependent on the integrity of the data, we verified the
469 data integrity in the next steps. The addition of poly(A)₂₀ (length of the reverse transcription
470 adapter) is sufficient to allow for the annealing of the poly(T)-adapter required for reverse
471 transcription and sequencing. This goes in line with the shortest median length we observed for
472 the 5S rRNA (see *E. coli* TEX sample) (see Supplementary Fig. 4). For most of the transcripts, a

473 poly(A) tail with 50 to 100 nt was detected. In addition, the overall correlation of transcript
474 abundances calculated from sequencing data using Nanopore or Illumina technology was very high
475 suggesting that a good coverage of the transcriptome was achieved and that native RNA
476 sequencing is not biased towards a subset of transcripts (see Supplementary Fig. 5a,b,c, transcript
477 abundance data in Supplementary Table 2).

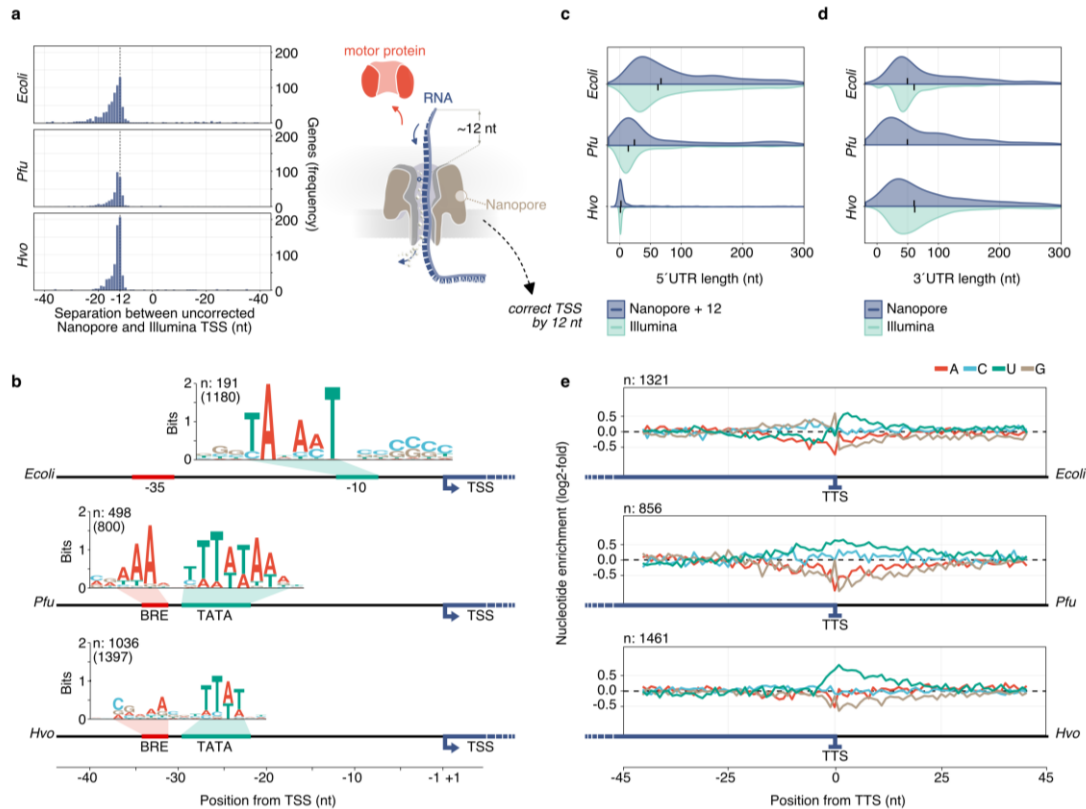
478

479 **Mapping of transcriptional boundaries**

480 *Transcription start sites*

481 Transcription start site (TSS) and transcription termination site (TTS) detection was based on the
482 determination of transcriptional units (TU) (compare material and methods section)³¹. In total, we
483 identified a comparably high number of TSS in ONT data sets compared to TSS detected by Illumina
484 d(ifferential) RNA-seq (see Supplementary Fig. 6a)^{29,32,33}. Furthermore, the substantial overlap of
485 genes with a predicted TSS in both technologies (see Supplementary Fig. 6a), allowed us to evaluate
486 the accuracy of ONT TSS mapping (positions of TSS derived from ONT TEX-treated samples in
487 Supplementary Table 3). For example, in case of *E. coli*, we could annotate the TSS for 1925 genes
488 using the results of a published dRNA-seq study, and 1,272 TSS were detected by ONT native RNA
489 sequencing. The portion of TSS identified only based on the ONT sequencing data (653 TSS) or
490 Illumina sequencing data (1,436 TSS) is mostly caused by the different algorithms used and the
491 limited sequencing depth in the ONT data sets. Strikingly, despite missing specific enrichment of
492 primary transcripts, the median 5' untranslated region (UTR) lengths were very similar when data
493 from ONT native and Illumina-based RNA sequencing were compared (*E. coli*: 68 ONT vs. 62
494 Illumina; *P. furiosus*: 23 ONT vs. 13 Illumina; *H. volcanii*: 1 ONT vs. 0 Illumina, Fig. 2b). Please note
495 that TSS-mapping based on Nanopore native RNA-seq data must be corrected by 12 nucleotides
496 (Fig. 2a,b). It has been observed previously that about 12 nt are missing at the 5' end of the
497 sequenced RNAs. This observation can be explained by a lack of control of the RNA translocation
498 speed after the motor protein falls off the 5' end of the RNA (Fig. 2a)^{66,67}.

499



500

501 **Figure 2 | Detection of transcript boundaries.** **a**, Left panel: Separation between uncorrected Nanopore-
 502 predicted TSS and comparison to Illumina d(ifferential) RNA-Seq data from published data sets for *E. coli*
 503 ²⁸, *P. furiosus*⁵³ and *H. volcanii*⁶⁰. Right panel: The translocation speed of the last 12 nucleotides (nt)
 504 is not controlled, as the motor protein is falling off. Therefore, native RNA reads are shortened by ~12 nt.
 505 **b**, Position of TSS is corrected for 12 nucleotides to calculate the length of 5' untranslated regions (UTR)
 506 in the Nanopore data sets (purple). 5' UTRs are compared to d(ifferential) RNA-Seq Illumina data sets
 507 (light-green). Median values are indicated by a black bar inside the distribution (compare Supplementary
 508 Fig. 6). **c**, Length of 3' UTRs is based on the prediction of transcription termination sites (TTS) and the
 509 comparison to annotated gene ends. Distribution of lengths is shown for Nanopore data sets (purple)
 510 and compared to Term-Seq Illumina data from *E. coli* and *H. volcanii* (light-green)²⁸. **d**, MEME analysis⁵³
 511 of extracted sequences upstream of Nanopore-predicted TSS reveals bacterial (position -10) and
 512 archaeal-specific promoter elements (BRE: B-recognition element, TATA: TATA-box recognized by
 513 transcription factor B), therefore validating the positions of predicted TSS. **e**, Nucleotide enrichment
 514 meta analysis was carried out by comparing the genomic sequences surrounding the TTS (-45 to +45) to
 515 randomly selected intergenic positions of the respective organism (n: 10000) (Terminator motifs in
 516 Supplementary Fig. 7).

517 Promoter analysis confirmed the presence of well-known sequence motifs of bacterial and
 518 archaeal promoters^{29,33,68}. This includes the TATA-box and TFB-recognition element (BRE)
 519 characteristic for archaeal promoters and the -10 element in bacterial promoters (Fig. 2d). The -
 520 35 element in *E. coli* has been previously shown to be less enriched compared to the -10 site⁵,
 521 which might explain why this element cannot be detected in the Nanopore data set. To analyse
 522 TSSs in more detail, we compared the 5' UTR lengths for all genes with predicted TSS in ONT and
 523 Illumina data sets (see Supplementary Figure 6b,c,d). The overall correlation between the two

524 techniques was high even though in some instances only a moderate correlation was found (see
525 Supplementary Fig. 6). As expected, the correlation improves with increasing sequencing depth for
526 a gene (>5 reads). While TEX-treatment is a common way of predicting TSS in Illumina sequencing,
527 we observed that it is not necessary for ONT data as very similar TSS are found in both TEX and
528 NOTEX data sets ($\rho = 0.86$) (see Supplementary Figure 6e).

529

530 *Transcription termination sites*

531 In prokaryotes, transcription termination is mediated either by a proteineous factor (Rho in
532 bacteria⁶⁹, CPSF in archaea⁷⁰) or intrinsic RNA sequences (bacteria: a GC-rich sequence that forms
533 a stem-loop followed by a U-rich sequence⁷¹, in archaea: poly(U) stretch⁵⁴). Native RNA reads are
534 sequenced in the 3' to 5' direction, which is a major advantage in the detection of termination sites
535 as any bias introduced after polyadenylation can be excluded. This approach opened up the
536 opportunity to not only map termination sites but to also gain insights into 3' UTR lengths, for
537 which no reference data sets for *P. furiosus* were available. The distribution of 3' UTRs in *E. coli*
538 and *H. volcanii* ONT data closely resembles the data from previous Illumina-based studies^{28,56}.
539 Strikingly, the length of untranslated regions at the 3' end of annotated transcripts is very similar
540 between the three prokaryotes (Fig. 2c). In total, 1321 TTS in *E. coli*, 856 in *P. furiosus* and 1461 in
541 *H. volcanii* were analysed (positions of TTS in Supplementary Table 4). A meta-analysis of all TTS
542 surrounding regions revealed different sequence-dependent termination mechanisms that were
543 confirmed using motif scanning and ΔG analysis (Fig. 2e, see Supplementary Fig. 7a-e). Our data
544 suggest that transcription in *P. furiosus* is terminated by a double-stretch of Uridines that are
545 distributed over a length of 22 nt, a finding that is in line with the terminator sequences detected
546 by Term-Seq in *S. acidocaldarius*⁵⁴ and similar to the U₍₈₎ sequence in *Thermococcus kodakarensis*
547 determined by an *in vivo* reporter assay⁷². The termination motif found in *H. volcanii* is a (U)₄-
548 sequence and located right after the TTS (see Supplementary Fig. 7d). In *P. furiosus*, the poly(U) is
549 not preceded by a stem-loop structure, confirming that stem-loop structures do not play a role in
550 hyperthermophilic organisms for general termination (see Supplementary Fig. 7e)^{54,73}. However,
551 this is less clear in *H. volcanii*, where stem loops have been shown to terminate transcripts,
552 although less efficiently (see Supplementary Fig. 7e)⁷³. The motif locations for both *Haloferax* and

553 *Pyrococcus* ONT sets suggest that accurate TTS detection of transcripts terminated by poly(U)
554 stretches is currently not possible. We observed that homopolymer sequences currently cannot be
555 basecalled accurately, which leads to problems during mapping and ultimately to TTS positions
556 that are positioned upstream of the poly(U) signal. This is also supported by a position-specific
557 comparison of TTS in *H. volcanii* identified with Illumina and ONT reads (see Supplementary Fig.
558 7f,g). However, it was encouraging to see, that with increasing sequencing depth the correlation
559 significantly improves (see Supplementary Fig. 7h). Analysing individual transcripts in *H. volcanii*
560 and *P. furiosus*, we found that a single transcript can exhibit diverse 3' ends. This is true for the
561 Pilin transcript in *H. volcanii* and the Histone A1 transcript in *P. furiosus*, respectively (see
562 Supplementary Fig. 8). Both genes are highly expressed and some transcripts carry extended 3'
563 UTRs. While the majority of transcripts are terminating at the first poly(U) stretch, a subset of
564 transcripts is substantially longer and terminate at subsequent poly(U) termination signals (see
565 Supplementary Figure 8). Interestingly, homogeneous short poly(U) signals are found both at the
566 canonical termination site and the termination site of the elongated 3'UTR in the case of the Pilin
567 transcript in *H. volcanii*. The same applies to the termination of the histone and Alba gene
568 transcripts in *P. furiosus* (see Supplementary Fig. 8). The histone transcript has already been
569 shown to terminate at four consecutive U-stretches (U1-U4) consisting of at least five U's *in vitro*⁴¹.
570 While we could confirm that the archaeal RNAP mainly terminates at the U1 site, the downstream
571 sites seem to deviate from the three U₅ backup TTS *in vivo*. Instead, termination already occurred
572 at two U₄ stretches, each upstream of U2 and U3, respectively (see Supplementary Figure 8d-f).
573 Surveying the heterogeneity of the transcripts with an extended 3'UTR, we found a heterogeneous
574 distribution in the length of the transcripts for both, the Histone and Alba mRNA. This pattern
575 suggests that either a step-wise trimming of the 3'UTR occurs that eventually yields the mature
576 RNAs or that the RNA polymerase reads through the first termination sequence, stochastically
577 stops transcription after the first termination sequence and RNA polymerases that continued
578 transcription beyond the first TTS terminate at one of the following TTS.

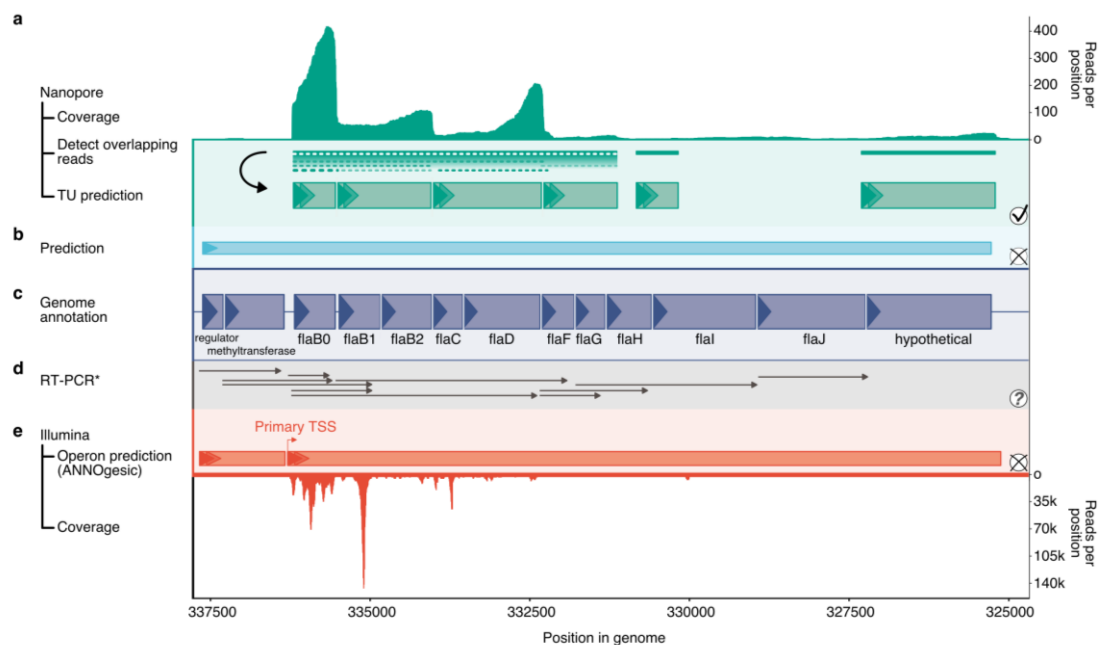
579 As observed for *E. coli* termination sequences, Cytosines are enriched over Guanosine adjacent to
580 the TTS in *P. furiosus* (Fig. 2e). Motifs detected in the *E. coli* data set correspond to intrinsic
581 (poly(U)) termination signatures and REP sequences^{74,75} that can frequently be found in intergenic
582 regions and cause transcription termination at Rho-dependent attenuators (see Supplementary

583 Fig. 7a,b)²⁸. As expected, fold stability analysis of intrinsic *E. coli* terminators and hairpin-forming
584 REP sequences, revealed secondary structures in both cases (Supplementary Fig. 7e). However,
585 the stem-loops could potentially also represent processing or pause sites.

586

587 Annotation of large transcriptional units

588 Long-read sequencing of native full-length RNAs has the potential to improve and facilitate
589 genome-wide transcriptional unit (TU) annotation, which can be visually explored in a genome
590 browser coverage track (Fig. 3a).



591

592 **Figure 3 | Transcription unit (TU) annotation of the flagellum-operon in *P. furiosus*.** **a**, Coverage of
593 Nanopore reads is shown in the top panel. TU prediction is performed by detection and linkage of
594 overlapping reads and splitting them according to a 3' drop in coverage (see Supplementary Fig. 8).
595 Predicted TUs are drawn with green boxes according to scale. **b**, Comparison to bioinformatical
596 prediction using the DOOR2 database⁶⁰. **c**, Genome annotation with abbreviated gene names, boxed
597 drawn to scale and strand indicated by triangles³³. **d**, Comparison to results from published RT-PCR
598 experiments⁷⁸. All transcripts detected are drawn by arrows. **e**, Operon prediction based on mixed
599 Illumina-Seq (coverage in lower panel) and predicted by ANNOgesic^{33,142}. The primary transcription start
600 site (TSS) of the large transcriptional unit is highlighted.

601 For whole-genome analysis, the annotation strategy was based on two major observations: First,
602 during RNA preparation, RNA processing or degradation can occur, which limits the probability of
603 sequencing an RNA in its native form as the percentage of full-length transcripts decreases with
604 expected gene size (see Supplementary Fig. 9a). Secondly, we detected a decrease in coverage from
605 the 3' to 5' end of the RNA in all RNA classes except for the spike-in control (see Supplementary

606 Fig. 9b), which is a limitation reported in the literature^{13,76,77}. Therefore, we assume that not
607 Nanopore sequencing but library preparation causes this problem. Based on this information, we
608 developed a strategy that first collapses all overlapping reads and then splits them according to a
609 significant coverage drop on the 3' ends (annotation of TUs based on this strategy in
610 Supplementary Table 5). We compared the results to database annotations and found that most of
611 the differences are either caused by the low sequencing depth or by single-unit operons that have
612 been collapsed and are now two-unit operons in the ONT data sets (see Supplementary Fig.
613 10a,b)^{31,60}. Even though limited read availability is a concern in all data sets, many large operons
614 were detected for all organisms (see Supplementary Fig. 10c). In case of limited bioinformatical
615 resources, TUs can be explored visually in a genome browser, which is mostly not possible for
616 Illumina reads (Fig. 3, see Supplementary Fig. 11,12). It further allows a quantitative analysis of
617 individual transcripts in relation to other elements of the TU and performs much better than pure
618 bioinformatical prediction or molecular biology methods (RT-PCR) as shown for the
619 flagellum/archaeillum operon in *P. furiosus* (Fig. 3)^{60,78}. Here, it was possible to (i) detect multiple
620 transcription units forming this cluster, (ii) confirm transcriptional start sites and (iii) to confirm
621 that flaB0, the protein that is referred to as the major archaeillin in *P. furiosus*^{2,6}, is transcribed in
622 large excess over the other archaeillum genes. The largest identified TU cluster in *H. volcanii* mainly
623 consists of ribosomal protein genes. Based on the native RNA-seq data, the analysis suggests that
624 this operon is split into two transcription units. This shows that the ONT native RNA sequencing
625 method provides the opportunity to annotate transcriptional units thereby outperforming the
626 bioinformatics-only prediction as well as the visual inspection of Illumina coverage (see
627 Supplementary Fig. 11). Besides, we confirmed the complex transcription pattern of the major
628 ribosomal protein gene cluster in *E. coli* that stretches over more than 10 kb, including the accurate
629 determination of TSS and TTS and a putative cleavage site in the *secY* gene (see Supplementary
630 Fig. 12)⁷⁹.

631 **Detection and confirmation of rRNA processing in *E. coli***

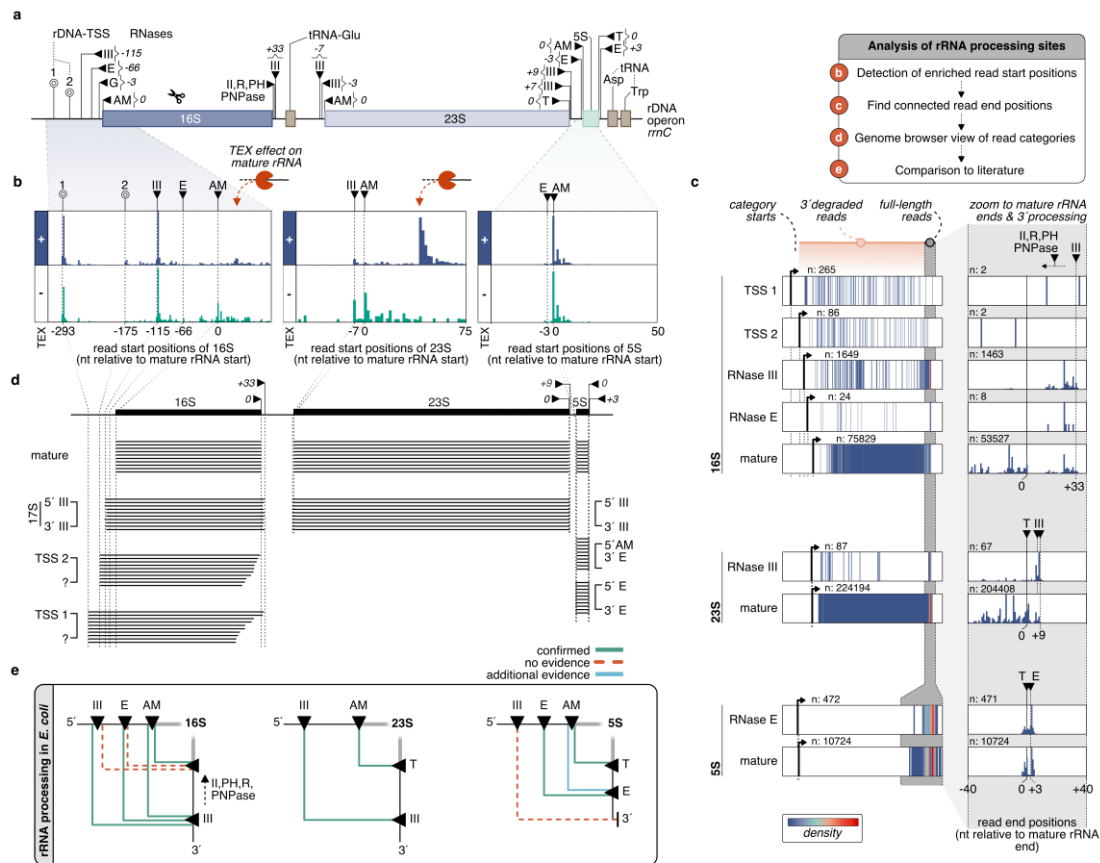
632 Next, we aimed to analyse the multi-step rRNA processing pathway which is the major RNA
633 maturation pathway in any prokaryotic cell. We first focus on the *E. coli* data set as the processing
634 of bacterial rRNAs is well characterized⁸⁰⁻⁸². Ribosomal RNA in *E. coli* is transcribed from 7

635 independent rDNA operons encoding the mature rRNAs (16S, 23S and 5S rRNAs) and some tRNAs
636 which are interspersed by RNA spacer elements⁸³. In agreement with a previous study,
637 transcription of *rrnC* from two promoters (transcription start sites at -293 and -175) was detected
638 accurately in the TEX-treated sample, which is enriched in primary transcripts (Fig. 4a,b)⁸⁴.

639 The rRNA maturation process, which requires the action of well-defined endo- and exo-
640 ribonuclease activities, culminates in the formation of stoichiometric amounts of mature 16S, 23S,
641 and 5S rRNAs^{80-82,85}. Unexpectedly, the sequencing efficiency of mature 16S rRNA was lower than
642 the 23S rRNA (Fig. 1b, see Supplementary Fig. 13). The reasons for this apparent discrepancy is so
643 far unclear.

644 To re-trace the multi-step rRNA maturation process, we performed a co-occurrence analysis of
645 read start and read end positions. Strikingly, we could identify most of the known 5'-
646 processing/intermediate sites at nucleotide resolution in wildtype *E. coli* (Fig. 4b). Next, we
647 categorized reads based on their experimentally verified and literature expected 5' terminal
648 positions and analysed 3'-enriched connected positions (Fig. 4c). Considering the 3'-to-5'
649 sequencing strategy of Nanopore sequencing, this co-occurrence analysis allows the assignment of
650 3' terminal positions and distinction to random 3' degraded reads.

651 Although we could detect RNA of similar size or longer (see above) very well, the short-lived full
652 rDNA operon transcript detected in RNase III deficient strain⁸⁶, is not observed using our
653 experimental set-up. In contrast, the downstream known pre-rRNA intermediates, which are
654 generated by the action of RNase III were detected (Fig.4). Among these intermediates, the 17S
655 pre-rRNA (115 additional nt at the 5' end and 33 nt at the 3' end of the 16S rRNA) and the P23S (7
656 additional nt at the 5' end and 8 nt at the 3' end of the 23S rRNA), were identified (Fig. 4b,c,d).
657 Final 5' end maturation of the 16S rRNA mainly occurs before the 3' end⁸⁰ by the action of
658 additional ribonucleases (RNase E -66, RNase G -3, RNase AM 0 5' mature⁸⁵), which leads to an
659 enrichment of reads that have extended 3' trailing regions compared to the mature position (Fig.
660 4c,d). Together we could identify most of the known rRNA processing-intermediates/-sites at
661 near-nucleotide resolution in wildtype *E. coli*. However, it should be noted that the current
662 experimental set-up can be biased by 5' and 3' degradation events, prohibiting precise 3' end
663 mapping in some cases and causing difficulties to identify short-lived/low-abundant pre-rRNA
664 intermediates.



665

666 **Figure 4 | Detection and confirmation of rRNA processing sites in *E. coli*.** **a**, Transcription of the rDNA locus
667 (rrnC) is starting from two promoters (transcription start sites at -293 and -175)⁸⁴. Precursor RNAs are
668 cleaved by RNases (black triangles) at depicted positions^{80,81,85,89}. **b**, Histograms of read start positions
669 for 16S, 23S and 5S rRNA. Positions are relative to the annotated boundaries of mature rRNAs and shown
670 for TEX (+, purple) and NOTEX (-, green) samples. **c**, Read start positions were used to classify categories and analyse the co-occurrence of read start to end positions. In the left panel, the color-coded density (low: blue, high: red) of read end positions from the category start position (black arrow) to the expected 3' terminal area (grey area) is shown for the selected categories. While all lines outside of the grey area presumably represent 3' degraded reads, the full-length read end positions inside the shaded area have been analysed in more detail in the right panel (only TEX sample is shown). **d**, Based on the co-occurrence analysis of enriched read start and end positions, single reads were extracted and are visualised in a genome-browser view. **e**, The action of endo- and exonucleases (black triangles) is required for the maturation of rRNAs in *E. coli*. The multi-step maturation process leads to intermediates we could confirm (green lines) using Nanopore sequencing. While red dashed lines indicate intermediate pre-rRNA we cannot detect, blue lines indicate the presence of an additional intermediate.

681

682 Insights into archaeal ribosomal RNA processing

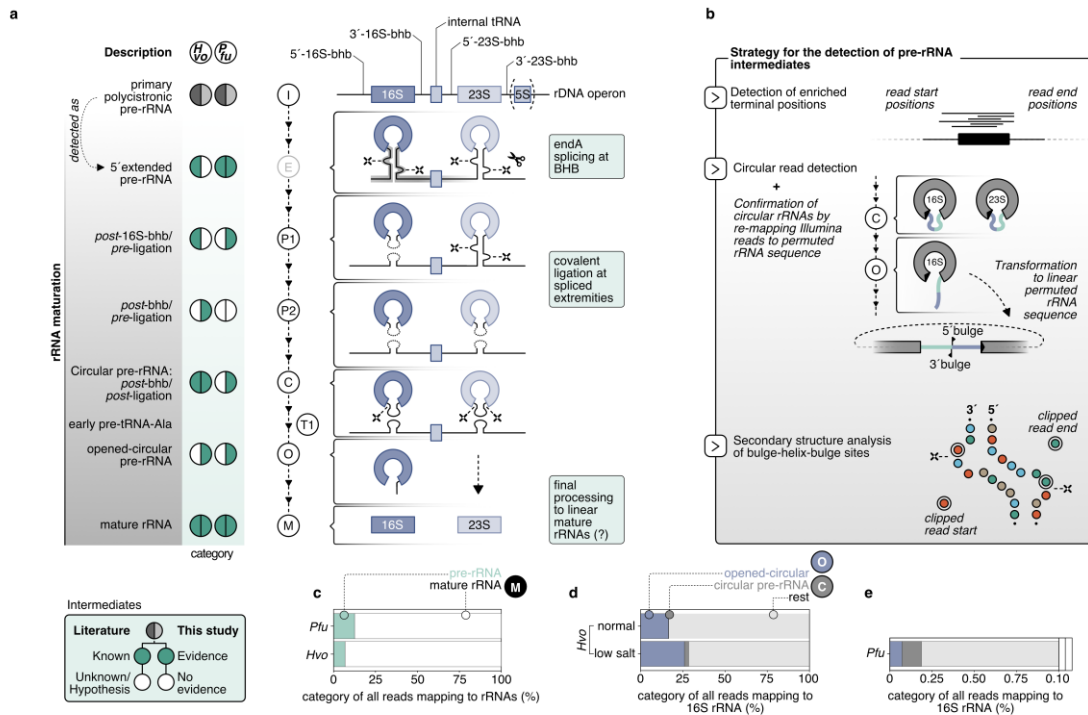
683 In comparison to bacteria or eukaryotes, ribosomal RNA processing in archaea is still poorly
684 understood⁸⁷⁻⁹⁰. Our current knowledge suggests that the primary polycistronic rRNA precursor
685 contains two processing stems formed by the 5' leader and 3' trailer sequences surrounding
686 16S and 23S rRNAs^{88,89,91,92}. In Euryarchaeota, the 16S and 23S rRNAs are additionally separated

687 by the presence of an internal tRNA. In most archaea, the 16S and 23S rRNA processing stems
688 contain a bulge-helix-bulge (bhb) motif which is, in the context of intron-containing tRNA,
689 recognized by the splicing endonuclease endA⁹¹⁻⁹³. Similar to intron-containing tRNA maturation,
690 processing at the bulge-helix-bulge motifs is followed by the covalent ligation of the resulting
691 extremities, thereby generating the archaeal specific circular pre-16S and circular pre-23S
692 rRNAs^{89,92,94,95}. The exact molecular mechanisms by which the circular pre-rRNA intermediates are
693 further processed into linear mature rRNAs remain to be fully characterized^{89,92,96}.

694 Performing enrichment analysis of terminal positions, we aimed to confirm and expand our
695 knowledge on the poorly characterized multi-step ribosomal maturation process in two
696 evolutionary divergent archaea, *P. furiosus* and *H. volcanii* (Fig. 5, see Supplementary Fig.
697 14)^{58,89,91,97}. As expected, almost all reads are categorized as fully matured transcripts of the
698 single 16S/23S rRNA cluster that do not contain extended 5' or 3' spacer regions (Fig. 5c).
699 Surprisingly, and in contrast to our analysis performed in *E. coli* (Fig. 4), some of the observed
700 mature rRNAs 5' positions did not precisely match the available annotations at NCBI
701 (<https://www.ncbi.nlm.nih.gov/genome/>) or the archaeal genome browser (AGB,
702 <http://archaea.ucsc.edu>), which are also showing discrepancies (summarized in Supplementary
703 Figure 14). However, selected examination of the putative mature rRNA extremities obtained by
704 ONT did match our independent experimental validations by primer extension analysis of the
705 5' ends of the 16S and 23S rRNAs of *H. volcanii* (Supplementary Fig. 14d). These results, and those
706 obtained for *E. coli*, suggest that the mature 5' of the rRNAs determined by native RNA sequencing
707 most probably represent the genuine mature rRNA extremities.

708 Despite the high sequencing depth of the (pre-)rRNA, we did not detect a full-length precursor
709 consisting of the 16S leading-16S-tRNA-23S-23S trailing elements in *P. furiosus* and *H. volcanii*,
710 suggesting that, similar to the *E. coli* situation (see above), very early rRNA processing events may
711 occur rapidly in these cells. The remaining rRNA reads were grouped according to (i) their 5'
712 leading and 3' trailing lengths, (ii) the number of junctions and (iii) clipping properties of the
713 alignments into several additional categories that are overall less abundant than the mature rRNAs
714 and may represent either rRNA processing intermediates or are RNA elements generated as a
715 product of pre-rRNA processing. Among these putative pre-rRNA-related intermediates, some are
716 common to both archaea analysed, whereas others are apparently only found in one or the other

717 organism. The pre-rRNA-related intermediates were selected on the basis of abundance and/or
 718 biological interpretability and/or prior characterization. The overall findings were used to extract
 719 an hypothetical rRNA maturation pathway in archaea which is summarized in Figure 5a. The
 720 rationale for the selected pre-rRNA intermediates for *H. volcanii* and *P. furiosus* is described in more
 721 detail below and exemplified in Figure 5b.



722

723 **Figure 5 | Update of the archaeal rRNA processing model.** **a**, The processing stems of the primary
 724 polycistronic pre-rRNA, formed by 5'-leader and 3'-trailer sequences, contain bulge-helix-bulge motifs
 725 that are recognized and cleaved by the endonuclease endA. This is followed by the covalent ligation of
 726 the resulting extremities, which leads to archaeal-specific circular pre-16S and pre-23S rRNAs. Further
 727 maturation steps are so far unknown. The multi-step maturation process was analysed based on the
 728 strategy depicted in b and compared to already known events. **b**, Strategy for the detection of pre-rRNA
 729 intermediates: Categories were first selected based on enriched terminal positions. Clipping
 730 abnormalities lead to the detection of circular reads that could be verified by re-mapping Nanopore and
 731 Illumina reads to a linear permuted rRNA sequence containing the joined 3'-to-5' bulge region. The exact
 732 position of the joined region was additionally verified by secondary structure analysis of the bulge-helix-
 733 bulge sites⁵⁵. **c**, Quantification of reads mapping to the mature rRNA (purple) and precursors (brown). **d**,
 734 Quantification of full-circular (green) and open-circular (orange) reads in *H. volcanii* wt and low-salt
 735 sample and in *P. furiosus*. The total number of these circular reads was compared to the number of reads
 736 mapping to the 16S rRNA.

737 In *H. volcanii*, we identified 3 classes of putative intermediates. In the first class (class P2) the pre-
 738 rRNA boundaries of these intermediates match the previously described bhb processing sites
 739 located within the 16S and 23S rRNA processing stems, respectively (see Supplementary Fig. 14).
 740 These intermediates extend from the 5' to 3' bulge cleavage sites, however, these extremities are

741 not covalently ligated and may correspond to post-bhb cleavage/pre-ligation pre-rRNA
742 intermediates. An exemplary verification of the 5' boundary of the post-bhb cleavage/pre-ligation
743 pre-23S rRNA analysed by primer extension is provided in Supplementary Figure 14d. The second
744 class (class C) correspond to permuted reads covalently connecting the 5' and 3' bulge cleavage
745 sites, and are likely observed as the result of random nicking of the circular pre-rRNA
746 intermediates during sample preparations and are categorized as post-bhb/post-ligation pre-
747 rRNA intermediates. We verified reads by re-mapping Nanopore and Illumina reads to a permuted
748 RNA sequence that was designed by joining the 3' bulge with the 5' bulge to mimic the actual
749 sequence of circular rRNAs (Fig. 5, see Supplementary Fig. 15). Similarly, we detected a third main
750 class (class O), which corresponds to a putative pre-16S rRNA intermediate showing an immature
751 3' end, which is extended by the typical permuted spacers sequence observed in the circular-pre-
752 16S rRNA⁹⁵. This topology possibly results from linearization of the circular pre-16S rRNA
753 intermediate at the mature 16S rRNA 5' end (opened-circular-pre-16S rRNA). This putative pre-
754 rRNA intermediate is relatively abundant in *H. volcanii* (n: 1120, 15% of all reads mapping in the
755 16S rRNA region) and strikingly shows a non random 3' end extremity - matching with the
756 linearization of circ-pre-rRNA at the mature 16S rRNA 5' end. In contrast, the resulting 5' end were
757 rather heterogenous, probably due to degradation during sample preparation (see Supplementary
758 Fig. 15b).

759 To provide additional examples that show the potential to describe rRNA processing events in
760 archaea, we sequenced an *H. volcanii* wildtype strain grown under low salt conditions known to
761 accumulate large amounts of a longer 16S rRNA variant (see Supplementary Fig. 14b,c)³⁰. Under
762 these conditions, a 16S rRNA (precursor) with extended 5' and 3' UTRs (5': -108 5' bulge, 3': +70
763 3' bulge) appears that is enriched in this context. Quantification by comparison with the NOTEX
764 wildtype set confirms the previous detection of this rRNA variant in a gel-electrophoretic analysis
765 of total RNA (see Supplementary Fig. 14b)³⁰. To reveal more details about the nature of these
766 precursors, we re-mapped the reads to the permuted linear rRNA 16S sequence. We observed that
767 the relative number of reads obtained for circ-pre-16S rRNA (class C) and especially of opened-
768 circ-pre-16S rRNA (class O) obtained under low salt conditions were exceeding the ones from
769 "normal" conditions, indicating that rRNA maturation and/or turnover is affected in this "stress"
770 condition (Fig. 5d). The functional relevance of these observations remain to be analysed.

771 In *P. furiosus*, for which we have obtained larger amounts of reads, we could define 4 categories of
772 pre-rRNA-related intermediates (see Supplementary Fig. 14k, ranked by their timely appearance):
773 (1) Fragmented full-length precursor rRNAs (I), (2) 16S rRNA leading/trailing sequence-tRNA-23S
774 rRNA, (3) a putative RNA chimera resulting from processing and RNA ligation activities that entails
775 the 16S rRNA leading/trailing sequence-tRNA-23S rRNA leading/trailing sequence (T1), and (4)
776 permuted 16S and 23S pre-rRNA intermediates (C) (Fig. 5, see Supplementary Fig. 14).

777 The putative permuted reads (4) are reminiscent of the reads typically observed for circular pre-
778 rRNA in *H. volcanii* (class C) and may correspond to the covalent ligation of the 5' and 3' spacers
779 generated by cleavages at the bulge-helix-bulge motifs within the processing stems (Figure 5 and
780 ^{92,94,95}). To verify this hypothesis, we performed RNA structure prediction of the corresponding
781 double stranded RNA regions (see Supplementary Fig. 16). In agreement with the permuted reads,
782 we could place the corresponding extremities within the bulge-helix-bulge motifs. However, the
783 23S processing stem does not adopt a canonical bhb motif, but forms an alternative structure
784 similar to the one previously described for the 16S rRNA bhb motif in *S. acidocaldarius*^{93,98}. Others
785 and we could previously demonstrate that this alternative structure is compatible with circular-
786 pre-16S rRNA formation in *S. acidocaldarius*^{94,95}. Therefore, these permuted reads likely originate
787 from random opening of the archaeal specific circular-pre-rRNA intermediates during sample
788 preparation/sequencing (as observed for *H. volcanii*) and suggest that like various archaea
789 analysed so far, circular pre-rRNA intermediates are also produced in *P. furiosus*. Although we
790 could detect a similar total number of circular pre-rRNA transcripts for *H. volcanii* and *P. furiosus*,
791 the proportion of this category with respect to all reads mapping to the 16S rRNA is very low, which
792 might reflect the actual abundance (Fig. 5e). However, considering the differing sequencing
793 efficiencies of the 16S rRNAs absolute quantifications cannot be made.

794 The early RNA chimera 16S rRNA leading/trailing sequence-tRNA-23S rRNA trailing sequence
795 precursor (T1) likely generated by cleavage and reciprocal ligation of the pre-16S and pre-23S
796 rRNAs at the predicted bulge-helix-bulge motifs were detected very accurately, and are
797 reminiscent of previous observations⁹² (Fig. 5, see Supplementary Fig. 14 l). Given the number of
798 reads, the direction of ONT sequencing from 3' to 5' and the accurate mapping, it is unlikely that
799 the additional putative rRNA precursor (P1) carrying the leading sequence in combination with
800 tRNA-23S rRNA is arising from an experimental artifact (Fig. 5, see Supplementary Fig. 14). In fact,

801 this variant is in good agreement with our recent *cis*-acting element analysis in *H. volcanii*⁹⁵ (see
802 also Discussion).

803 Taken together, our analysis confirms and expands the number of putative pre-rRNA
804 intermediates in archaea. Moreover, this extended framework provides an additional basis to
805 facilitate further definition of common and specific principles of rRNA maturation in archaea.

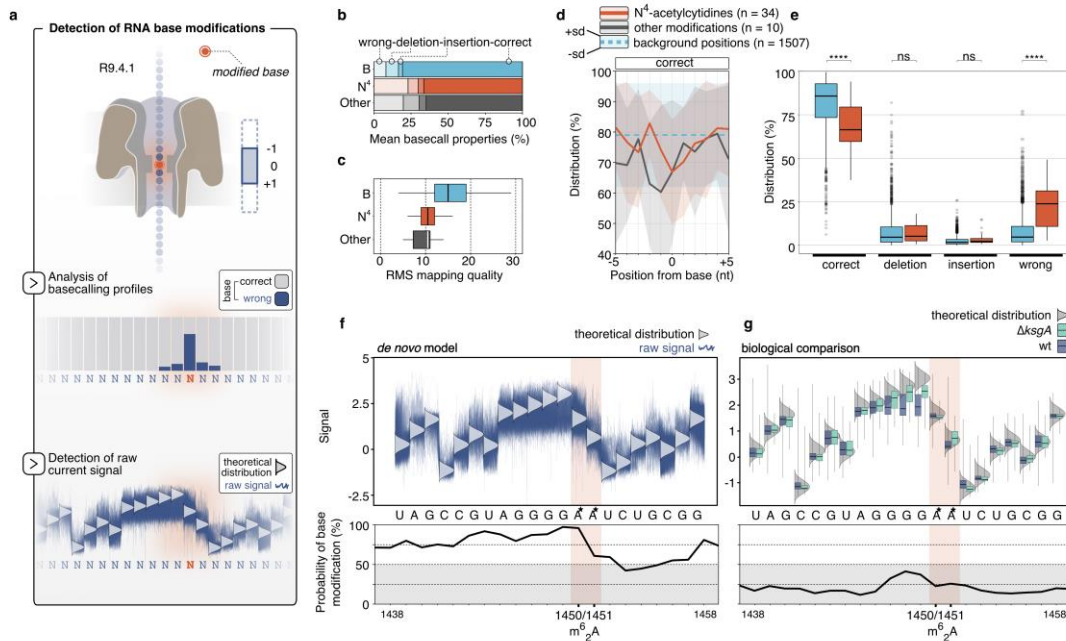
806

807 **Towards mapping of RNA base modifications**

808 More than 160 types of modified bases have been described in RNAs so far⁹⁹. In contrast to other
809 sequencing techniques, Nanopore-based sequencing offers the possibility to detect base
810 modifications directly as these modifications lead to an electric current signal that differs from the
811 expected theoretical distribution obtained by the unmodified nucleotide sequence^{15,16,20,100}. In
812 turn, these signal changes might also lead to differences in the basecalling profiles (e.g. systematic
813 errors or a drop in basecalling quality). Approaches based on signal deviations or basecalling
814 errors have already been applied to map RNA and DNA modifications in different organisms.
815 However, accurate *de novo* RNA modification prediction with single-nucleotide resolution is still
816 challenging as more than one base affects the current through the pore (see Fig. 6a). In addition,
817 current deviation is influenced by the type of modification and the surrounding sequence
818 context¹⁰¹.

819 Despite these limitations, we aimed to study rRNA modifications in archaea and explored different
820 analysis strategies (Fig. 6). Based on the approaches mentioned above, we benchmarked the
821 potential to detect known and putative modification sites in the 16S rRNA. We focused first on the
822 16S rRNA modifications of *P. furiosus*, using the recently established 16S rRNA modification
823 pattern in the close relative *Pyrococcus abyssi*⁵⁹. This set includes 34 N⁴-acetylcytidines, and 10
824 other modifications of diverse types⁵⁹. Compared to a background set consisting of all other
825 positions in the *P. furiosus* 16S rRNA, we observed that the surrounding sequencing context of all
826 modified bases is significantly enriched in basecalling errors (Fig. 6b) and also had a comparatively
827 low mapping quality (Fig. 6c). Depending on the type of modification (acetylation vs. diverse),
828 these metrics looked very different across a sequence context from -5 to +5 from the exact position
829 of the modified base (Fig. 6d, see Supplementary Fig. 17a,b). While N⁴-acetylcytidines were mostly

830 miscalled at their predicted position, the other diverse base modifications had various effects on
 831 all metrics (Fig. 6b, see Supplementary Fig. 17a,b). Using the position information derived from *P.*
 832 *abyssi*, our analysis suggest that the putative N⁴-acetylcytidine modification leads to a wrong base
 833 assignment during basecalling (Fig. 6d,e). In fact, this systematic non-random error was also
 834 reflected by the high proportion of a central T instead of C in the CCG context of the acetylation
 835 (see Supplementary Fig. 17c,d).



836

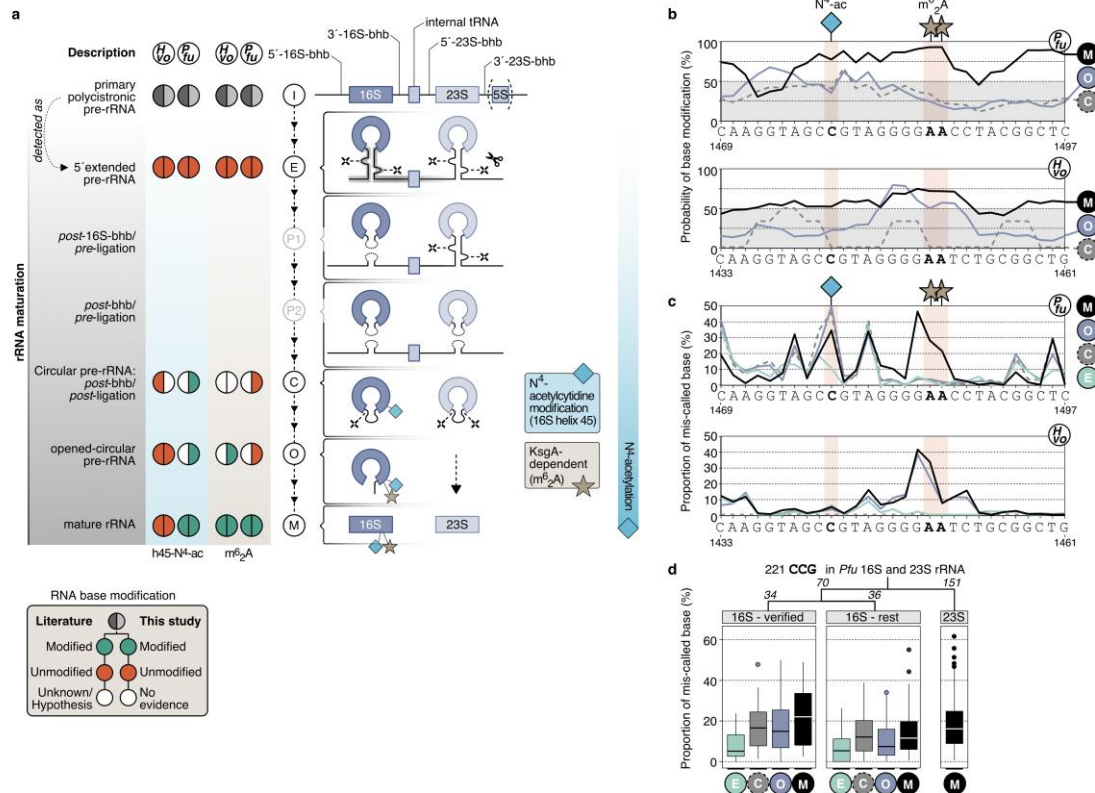
837 **Figure 6 | Detection of RNA base modifications in archaeal 16S rRNA based on basecalling and raw signal**
 838 **profiles.** **a**, In the R9.4.1 pore more than one base affects the current through the pore. RNA base
 839 modifications can be predicted as the modification might alter the raw signal which can in turn influence
 840 the basecalling profile. The performance of the two strategies was evaluated for potentially present N⁴-
 841 acetylations in *P. furiosus* (**b-e**, basecalling properties) and the KsgA/Dim1-dependent dimethylation
 842 (m⁶A) in *H. volcanii* (**f, g**, raw current signals). **b**, Analysis of mean basecall profiles of N⁴-acetylated
 843 positions (red), diverse other modifications (grey) and all other positions of the 16S rRNA in *P. furiosus*.
 844 The properties (wrong, deletion, insertion, correct) are shown by different transparencies. **c**, The root
 845 mean square (RMS) mapping quality gives an estimation of the overall mapping quality and is shown for
 846 the defined position categories in **b**. **d**, The proportion of correct basecalls is shown in a window from -
 847 5 to +5 from the presumably modified/or background base. Shaded areas show the upper and lower
 848 standard deviation, while the lines show the mean values. **e**, Distribution of basecall properties for the
 849 34 N⁴-acetylcytidines. Statistical significance (p-values, T-test) is indicated by asterisks (p-value > 0.05: ns
 850 (not significant), p <= 0.0001: ****). **f**, Raw signal of reads (blue squiggles) mapping to 16S rRNA in *H.*
 851 *volcanii* are compared to the theoretical distribution of native non-modified RNA (grey distribution) using
 852 the *de novo* detection model in tombo in the upper track.⁵⁷ The m⁶A modification at position 1450/1451
 853 (from 16S start) is indicated by an asterisk in the sequence track. The probability of each base to be
 854 modified (in %) is calculated and shown in the lower panel for the selected sequence. **g**, Position-specific
 855 boxplot comparison of signals from sequences surrounding the m⁶A modification in *H. volcanii* wildtype
 856 (blue) and the ΔksgA mutant. The theoretical distribution of read signal is indicated by a grey distribution
 857 curve for every base. The probability is computed based on the comparison of the two samples.

858

859 To analyse whether these modifications are already established at early steps of rRNA maturation,
860 we looked at the basecalling properties of 5'extended pre-rRNAs and compared them to mature
861 16S rRNA. Importantly, we did not observe significant basecalling errors in these selected
862 precursor rRNAs (5'extended pre-16S RNA) indicating that the cytidine N⁴-acetylation is not
863 occurring early in the rRNA maturation pathway (see Supplementary Fig. 17e) (see below for
864 further details).

865 As the approach based on systematic errors gave us promising results for N⁴-acetylations, but were
866 less unambiguous for diverse modifications, we wanted to evaluate the potential to detect RNA
867 base modification from raw signals using Tombo (Fig. 6a, updated Tombo version from Stoiber et
868 al.⁵⁷). To this end, we first focused on the dimethylation (m⁶2A) introduced by the enzyme
869 KsgA/Dim1 at position A1450/A1451 in *H. volcanii* (A1518/A1519 *E. coli* numbering)^{58,102}. Using
870 the *de novo* model in Tombo the calculated probability of a modification was very high for the
871 stretch of Guanosines adjacent to position A1450 (Fig. 6f). Mapping to single-nucleotide resolution
872 is difficult as more than one base contributes to the actual electric current signal in the
873 nanopore¹⁰³. In the next step, a comparison of a wildtype sample to a deletion mutant of archaeal
874 KsgA/Dim1 homologue helped us to confirm that the current signal alteration in this particular
875 region is dependent on the KsgA/Dim1 m⁶2A modifications and not the homopolymer-G-stretch
876 (Fig. 6g). The analysis further revealed a reduced signal variability at non-modified positions
877 between the two samples in comparison to the theoretical distribution, which leads to less false
878 positives in the statistical analysis and highlights the benefits of a background read model.

879 Assuming that early pre-rRNAs represent a state where base modifications are not yet
880 quantitatively introduced, we used these reads as a background model to explore the potential to
881 detect the introduction of base modifications at different stages of rRNA maturation in archaea.
882 Therefore, we generated multiple sets by sorting reads according to the main classes of pre-rRNA
883 intermediates described above for *H. volcanii* and *P. furiosus* (Fig. 7a). For *H. volcanii* and *P. furiosus*,
884 we compared 5'extended 16S rRNA, circular pre-16S rRNA, opened circular-pre-16S rRNA and
885 mature 16S rRNA. We first focussed on analysing the m⁶2A and N⁴-acetylcytidine signatures across
886 the putative different stage of rRNA maturation in archaea. To this end, we evaluated basecalling
887 and raw signal profiles using the 5' extended pre-rRNA as a background model as the former
888 performed well for N⁴-acetylcytidines, while the latter for m⁶2A detection.



889

890 **Figure 7 | Detection of RNA base modifications at different stages of rRNA maturation in archaea.** **a**, During
 891 the maturation of ribosomal rRNAs base modifications are introduced at different time points. While the
 892 the KsgA/Dim1-dependent dimethylation (m⁶2A) is proposed to function as a quality control during late
 893 biogenesis (mature and open-circular pre-rRNA), N⁴-acetylations in *P. furiosus* seem to be added
 894 successively during rRNA maturation. **b**, Probability of base modifications calculated by the tombo
 895 sample-compare approach using 5'-extended pre-rRNAs as a background model for *P. furiosus* (upper
 896 panel) and *H. volcanii* (lower panel). The approach was applied to mature (M, black), open-circular (O,
 897 purple) and circular pre-rRNAs (C, grey). The illustration shows the sequence region of the 16S rRNA
 898 containing the N⁴-acetylcytidine modification in helix 45 and the dimethylation. **c**, The basecalling profile
 899 of the same section was analyzed during the maturation stages. The proportion of the respective base to
 900 be mis-called (category wrong) is shown for categories M, O, C and 5'-extended pre-rRNAs (E, green). **d**,
 901 Comparison of the proportion of mis-called based for all CCGs detected in the 16S and 23S rRNA in *P.*
 902 *furiosus*. 34 positions have been experimentally verified in *P. abyssi* and are potentially also present in *P.*
 903 *furiosus*⁵⁹.

904 Basecalling anomaly in the m⁶2A region was detected within the mature 16S rRNA of both *P.*
 905 *furiosus* and *H. volcanii*, and could be confirmed by a high probability of base modification around
 906 this positions using the tombo model (Fig. 7b,c, see Supplementary Fig. 18). Interestingly, similar
 907 profiles were detected for the putative opened-circ-pre-16S rRNA in *H. volcanii*, but not in *P.*
 908 *furiosus*. This finding is in line with a proposed “quality control” function of KsgA/Dim1 during late
 909 biogenesis of the small ribosomal subunit¹⁰⁴⁻¹⁰⁶. Similarly, we analysed N⁴-acetylcytidine known
 910 to occur in the vicinity of the m⁶2A. However, this modification occurs prior to the KsgA/Dim1-
 911 dependent modification during eukaryotic ribosome biogenesis¹⁰⁷⁻¹¹¹. In agreement with previous

912 analysis⁵⁸, no apparent N⁴-acetylcytidine modification was observed at the equivalent position in
913 *H. volcanii* (Fig. 7c). In contrast, an increase in base-calling errors at the expected position was
914 observed in circular pre-rRNAs and mature 16S rRNA, but not within 5' extended pre-16S rRNA in
915 *P. furiosus*. Therefore, and similarly in eukaryotes, N⁴-acetylcytidine modification in helix 45
916 precede the KsgA/Dim1-dependent m⁶₂A modifications in *P. furiosus*. Note that the results for the
917 circular pre-16S rRNA (grey, Fig. 7) should be taken with care in *H. volcanii*, given the limited
918 number of reads in this category (see Supplementary Fig. 18). However, it is tempting to speculate
919 that a different timing of events in *H. volcanii*, observed by the earlier m⁶₂A modifications, is caused
920 by the absence of N⁴-acetylations.

921 To further extend on the timely order of all N⁴-acetylcytidine modification potentially present in *P.*
922 *furiosus*, we analysed the basecalling profiles across different rRNA maturation stages (Fig. 7d). In
923 addition, we compared it to all other CCGs that are present in 16S and 23S rRNA as N⁴-acetylation
924 have been shown to be introduced in a CCG context in *P. abyssi*⁵⁹. This analysis suggests that (i) N⁴-
925 acetylcytidine modifications may be also scattered across the 23S rRNA sequence, and (ii) these
926 modifications are established in the course of pre-rRNA maturation (circ-pre-rRNA in Figure 7d).
927 Taken together, our analysis, suggests that despite the current limitations, ONT allows to
928 discriminate (some) rRNA modifications across selected rRNA maturation events. Moreover, these
929 data support the long-standing hypothesis that hyperthermophilic organisms might stabilize their
930 rRNAs by a higher degree of RNA modifications^{112,113}.

931

932

933 Discussion

934 Performing whole-transcriptome native RNA-seq study in prokaryotes provided us with a wealth
935 of information on transcriptional and post-transcriptional processes in *E. coli* and the archaeal
936 model organisms *H. volcanii* and *P. furiosus*. Here, we will mostly discuss new biological insights
937 that emerged from our study. Additionally, we will reflect on the advantages and disadvantages of
938 Nanopore native RNA-seq.

939 Insights into transcriptional processes

940 Bacterial and archaeal transcription is an intensely studied molecular process and the mechanisms
941 of basal transcription are well understood¹¹⁴. Native RNA sequencing allowed us to retrieve
942 accurate information of transcript boundaries on both 5' and 3' ends. Our data show that 3' UTRs
943 length distributions are comparable between *E. coli*, *P. furiosus* and *H. volcanii* with the majority of
944 mRNAs showing a length between 30-70 nt. Similar to bacteria, archaea encode a large number of
945 small non-coding RNAs¹¹⁵. However, many regulatory events that involve the regulation via small
946 RNAs take place at bacterial 5' UTRs¹¹⁶. We and others found that 5' UTRs are significantly shorter
947 in many archaea supporting the idea that post-transcriptional regulation is mediated via the 3'
948 rather than the 5' UTR in these groups¹¹⁷. Additionally, we determined transcription termination
949 sites, which are well analysed for bacterial species but only a few studies focused on archaeal
950 termination mechanisms, especially on the genome-wide level. In both archaeal species studied,
951 poly(U) stretches were overrepresented at termination sites agreeing well with termination
952 sequences found in *Sulfolobus* and *Methanosarcina*⁵⁴. Interestingly, the majority of TTS found in
953 *Pyrococcus* transcripts is composed of two U-stretches with at least five consecutive uridine bases
954 while a subclass of *Haloferax* transcripts is almost exclusively terminated by a single U-stretch with
955 four uridine bases. It has been shown that a five base U-stretch is sufficient to induce termination
956 *in vitro*^{72,118,119}. Similar observations were described in a recent study by Berkemer et al, which
957 identified a poly(U)₄ stretch to be the termination signal in intergenic regions^{56,59}. Notably, the *H.*
958 *volcanii* genome is distinguished by a high GC content leading to a low probability for the occurrence
959 of U₅ stretches and hence, the transcription machinery might have adapted to recognise U₄
960 stretches as termination signal. However, the current data set suggests that this short termination

961 signal might be a specific feature for a subclass of *Haloferax* transcripts resembling the poly(U)
962 termination motif found in *E. coli*. All other archaeal organisms (*P. furiosus*, *M. mazei*, *S.*
963 *acidocaldarius*) investigated so far terminate transcription at multiple consecutive poly(U)
964 stretches. Possibly, *Haloferax* relies on additional termination signals or yet unknown termination
965 factors. A putative candidate is archaeal CPSF1 (aCPSF1, also known as FttA), a recently described
966 archaeal termination factor^{70,120} that is widespread in archaea. aCPSF1 acts as ribonuclease that
967 was shown to cleave transcripts after a poly(U) stretch to trim transcripts and facilitates
968 transcription termination in *Thermococcus kodakarensis*⁷⁰ and *Methanococcus maripaludis*¹²⁰. The
969 arising 3' UTR isoforms were detected using Term-seq analysis¹²⁰. We also observed heterogeneity
970 in the case of the Pilin and histone transcripts, respectively, that are distinguished by varying
971 lengths of the 3' UTR suggesting that aCPSF1 might trim a subset of genes in *H. volcanii* and *P.*
972 *furiosus*. It is noteworthy that 3' UTR isoforms were also detected in Term-seq studies with
973 *Sulfolobus* and *Methanosarcina*⁵⁴. However, in contrast to the Pilin, Alba and histone transcripts,
974 the 3' UTR isoforms arise from termination at different sites of a single continuous poly(U) stretch
975 suggesting that the isoforms arise from a stochastic termination process of the RNA polymerases
976 at an extended poly(U) stretch at the end of the gene. The gradual termination observed in this
977 study might also be influenced by the coupling of transcription and translation. These genes are all
978 highly expressed and translated. Hence, it seems plausible that the ribosome is efficiently coupled
979 to the RNAP¹²¹ (as observed in bacteria^{38,38,122,123}). Several studies in bacteria showed that the
980 ribosome influences transcription (and *vice versa*)^{124–126}. The stochastic termination might
981 therefore be a result of the uncoupling of the ribosome at the end of the mRNA potentially also
982 inducing the dissociation of the transcription elongation complex. Taken together, these data
983 suggest that a variety of termination mechanisms (that can even co-occur in the same cell) can be
984 found in archaea ranging from stochastic intrinsic termination at extended poly(U) stretches
985 (*Pyrococcus*, *Sulfolobus*, *Methanosarcina*), to abrupt termination at short uridine tracts (*H. volcanii*)
986 and factor-dependent termination that results in trimming of the 3'UTR (*H. volcanii*, *P. furiosus*, *M.*
987 *maripaludis*, *T. kodakarensis*).

988 In the context of transcription, the long and overlapping native RNA reads helped us to analyse the
989 transcriptional landscape at multigene operons. More specifically, we focused on the archaeal

990 flagellum (archaellum) operon, encoding for the archaeal motility machinery¹²⁷, as the
991 transcription unit assignment remained ambiguous so far⁷⁸. In contrast to bioinformatical and
992 Illumina RNA-seq-based predictions and attempts to unravel the TU via primer extension
993 experiments, we found that the archaellum operon in *P. furiosus* is transcribed in multiple units
994 with highly diverse abundances. The *flaB0* gene encodes the major archaellin/flagellin protein that
995 forms the filament of the archaellum and therefore, the organism has to produce this protein in
996 large quantities as apparent from the expression level⁷⁸. Interestingly, FlaD mRNA is expressed at
997 comparably high levels as well supporting the idea that FlaD is a major constituent of the
998 archaellum in *P. furiosus*. It has been speculated that FlaD forms the cytosolic ring of the archaellum
999 that anchors the filament in the outer membrane¹²⁸. The identity and functional role of FlaD are,
1000 however, not known so far.

1001 **Insights into rRNA processing in archaea**

1002 In this study, we have assessed the suitability of native RNA sequencing to obtain information on
1003 the rRNA maturation pathway of different prokaryotes. Ribosomal RNA processing proceeds via
1004 the coordinated and defined order of ribonucleases action (exonucleolytic and/or endonucleolytic
1005 cleavages) which generate pre-rRNA intermediates with defined premature rRNA
1006 sequences^{82,90,129,130}. The establishment of faithful rRNA maturation maps in model organisms, like
1007 *E. coli*, *S. cerevisiae* or human cell culture has required numerous analyses over the past
1008 decades^{82,90,129,130}, and remains a technical challenge. Therefore, methodologies that might
1009 accelerate the systematic analysis of rRNA maturation pathways across the tree of life, thereby
1010 enabling to unravel the diversity of rRNA processing strategies need to be established. Beyond the
1011 identification of processing sites, the order of the processing events which can be, in part, deduced
1012 from co-occurrence analysis of the 5' and 3' extremities is of biological relevance^{82,90,129,130}.
1013 Whereas we could confirm and extend our general view on the rRNA maturation pathway in
1014 archaea, the 3'-5' processivity of Nanopore native RNA sequencing observed for rRNA and the
1015 potential RNA degradation during sample preparation impedes the accurate quantitative analysis
1016 of pre-rRNA extremities co-segregation (see Fig. 5 and Supplementary Fig. 9b). Nevertheless, we
1017 could, in most of the cases, confirm and expand the presence of pre-rRNA intermediates and
1018 processing sites in the different organisms analysed, including the archaeal specific circular-pre-

1019 rRNA intermediates^{89,92,94-96}(see discussion below). Together our findings are summarized into an
1020 updated archaeal rRNA processing model described in figure 5 and are discussed below.

1021 The full length theoretical primary rRNA transcript was not identified in any of the archaeal
1022 organisms analysed. Similarly, this primary rRNA is generally difficult to observe in wildtype *E. coli*
1023 (^{86,131} and this work). Collectively, these observations suggest that short-lived and/or low
1024 abundant pre-rRNA intermediates escape the detection capacity of the current experimental set-
1025 up. Accordingly, it is also difficult to infer differences in rRNA processing features between
1026 different (archaeal) organisms by virtue of observed pre-rRNA intermediates absence/presence
1027 pattern. In fact, these differences may also be related to organism-specific changes in pre-rRNA
1028 intermediates relative levels, which will depend on the sum of the reaction kinetics of the different
1029 maturation steps in a given condition.

1030 Among the identified pre-rRNA intermediates, the *post*-16S-bhb/*pre*-ligation precursor (P1),
1031 which is observed in *P. furiosus* and includes ligation at the bhb motif of the upstream region of the
1032 16S leader and downstream region of the 16S trailer sequences and continues to the downstream
1033 tRNA/23S sequences, is of particular interest (see Supplementary Fig. 14k). The presence of this
1034 ligation event suggests that the 16S rRNA bulge-helix-bulge processing occurs prior to internal
1035 tRNA and 23S rRNA maturation. Although, this ligation event was not identified by ONT in *H.*
1036 *volcanii*, this observation is in agreement with our recent functional *cis*-acting element analysis
1037 performed in *H. volcanii*^{89,92,94}. In fact, based on this previous analysis we have proposed a model
1038 by which 16S rRNA maturation proceeds and is required for the downstream maturation of the
1039 internal tRNA and 23S rRNA. Moreover, we have hypothesized that ligation of the 16S rRNA
1040 leader/trailer resulting from the 16S rRNA bulge-helix-bulge maturation process generates a
1041 putative new pre-rRNA intermediate for which the corresponding ligation event could be observed
1042 in *Pyrococcus furiosus* using native RNA sequencing⁹⁵. In addition, the presence of an RNA chimera
1043 containing the leading/trailing/tRNA parts (T1) (*post*-bhb/*post*-ligation) support the idea that the
1044 maturation of the co-transcribed internal tRNA is inefficient or inhibited and may preferentially
1045 occur after processing of the 16S and 23S rRNA bulge-helix-bulge which liberate the circular pre-
1046 16S and pre-23S rRNAs (C) (suggested in^{92,95}, and this work). The presence of circular pre-16S and
1047 pre-23S rRNAs and their processing sites could be verified and established in *H. volcanii* and *P.*
1048 *furiosus*, respectively (Fig. 5, see Supplementary Fig. 15/16). Recently, we determined the

1049 functional requirement of the bulge-helix-bulge motifs for the formation of circ-pre-rRNAs in *H.*
1050 *volcanii*. Moreover, in analogy to intron containing-tRNA splicing, the rRNA bhb motifs are
1051 presumably cleaved by the tRNA splicing endonuclease (endA) prior to covalent
1052 circularization^{91,95,96}. Although intact circular RNA can not be directly sequenced by ONT, we
1053 noticed the presence of permuted transcript in *H. volcanii* corresponding to the ligation events
1054 previously identified for circ-pre-rRNAs in *H. volcanii*⁹⁵. Most of these permuted reads were also
1055 showing random and heterogenous 5' and 3' ends thereby suggesting that these pre-rRNAs were
1056 likely the result of randomly nicking of circular pre-rRNA intermediates during sample
1057 preparation (see Supplementary Fig. 15). Noteworthy, similar permuted reads were observed in
1058 *P. furiosus*, for which the presence of circular-pre-rRNA intermediates is not established thus far.
1059 Whereas, the observed ligation could be accurately mapped to the predicted 16S bhb motif, the
1060 23S bhb motif could not be accurately predicted (data not shown). However, our manual
1061 inspection suggests that the permuted reads extremities match to an imperfect, presumably less
1062 stable, bhb motif within the 23S processing stem (see Supplementary Fig. 16b). This property is
1063 reminiscent to the "aberrant" 16S bhb motif used for circular-pre-16S rRNA formation in *S.*
1064 *acidocaldarius*^{93-95,98}. Whether these structural features are stabilized by additional factors or
1065 enable a certain degree of regulation during the rRNA maturation process in the cellular context is
1066 unknown.

1067 In addition to the circular pre-rRNAs, we observed pre-rRNA intermediates cleaved at the bhb
1068 motifs but not yet ligated into circular pre-rRNA in *H. volcanii* (*post-bhb/pre*-ligation pre-rRNAs)
1069 (P2). Whereas, the presence of this intermediate processing step is theoretically expected, they
1070 were only detectable in *H. volcanii* (see Fig. 5a, see Supplementary Fig. 14), suggesting that the
1071 maturation kinetics or stability of these pre-rRNA intermediates varies among these organisms.

1072 How the circular pre-rRNAs are further processed into linear mature rRNA is not well understood.
1073 Based on our current knowledge, several non-mutually exclusive hypothesis can be drawn: (i)
1074 opening of the circular-pre-rRNA within the ligated spacer region and subsequent maturation of
1075 the 5' and 3' end; (ii) opening of the circular pre-rRNA by first maturation of the 5' end mature rRNA
1076 followed by 3' end maturation; or (iii) opening of the circular pre-rRNA by first maturation of the
1077 3' end mature rRNA followed by 5' end maturation. A category of putative 16S pre-rRNA
1078 intermediates observed in *H. volcanii*, may provide some indications how linearization of the

1079 circular pre-16S rRNA is achieved. In fact, this particular intermediate was extended in its 3' end
1080 by the presence of the ligated 5' and 3' spacers normally observed in the circular pre-16S rRNAs
1081 and this 3' extension consistently ended just prior to the 16S 5' mature ends. This particular
1082 configuration is suggestive of 5' end maturation of circular-pre-16S rRNA prior to final 3' end
1083 maturation, thereby generating opened-circular pre-16S intermediates (O) (see Supplementary
1084 15b). Although the majority of opened-circular pre-16S rRNAs is degraded from its 5' end, we
1085 detected a subset representing the theoretical full length (see Supplementary Fig. 15b,c).
1086 Additional properties of this putative intermediate is in agreement with its positioning during
1087 rRNA maturation (see below discussion on rRNA modifications) and with the prevalence of 16S
1088 rRNA 5' maturation prior to its 3' end previously observed in bacteria and eukaryotes^{82,90}. Overall,
1089 future functional characterization of the *cis*- and *trans*-acting elements required for pre-rRNAs
1090 maturation will be necessary to further refine our view on archaeal rRNA processing.
1091 In conclusion, despite some intrinsic limitations, we provide evidence that direct RNA sequencing
1092 technologies can be a useful tool to approach intricate maturation pathway like rRNA maturation,
1093 and expand our understanding of RNA maturation in prokaryotes.

1094

1095 **Towards the mapping of rRNA modification patterns**

1096 RNA modifications have been described already in the 50-60s, and have gained significant
1097 attention over the last years, under the generic term of the epitranscriptome¹³²⁻¹³⁴. The high-
1098 throughput analysis of these post-transcriptional modifications remains challenging and mostly
1099 relies on indirect methods, like primer extension stops analysis and/or chemical
1100 recoding/derivation strategies^{135,136}. Native RNA sequencing may fill an important gap to
1101 systematically analyse RNA modifications on a genome-wide scale. However, global strategies
1102 enabling the faithful determination of RNA modification identity and position needs to be
1103 developed. Several recent analyses have explored different strategies to evaluate the capacity of
1104 ONT to accurately detect RNA modifications (e.g. m⁶A)^{15,16,65,137,138}.

1105 RNA modifications can lead to electric current signals varying from the theoretical signal expected
1106 for the unmodified canonical ribonucleotides. These properties can be harnessed, on the one hand,
1107 to predict RNA modification probability by comparing theoretical and experimental electric
1108 current signal distribution, and on the other hand, variation of electric signals may increase the

1109 rate of basecalling errors. In both cases, the comparison of the profiles to a background distribution
1110 of non-modified nucleotides leads to a significant reduction of false-positives. We evaluated the
1111 potential to use early rRNA precursors, which are expected to contain incomplete modification
1112 patterns, as a background model and applied this strategy to analyse different stages of rRNA
1113 maturation.

1114 To validate our approach, we first focussed on two types of modification occurring in close
1115 proximity in helix 45 of the 16S/18S rRNA, but at distinct stages of rRNA maturation, namely the
1116 almost universally conserved KsgA-dependent dimethylations (m⁶₂A) and the less conserved
1117 Kre33/Nat10-dependent N⁴-cytidine acetylation^{16,102,105,139,140}. By analysing basecalling profiles
1118 and raw signals in wt and KsgA deletion strain we could unambiguously provide *in vivo* evidence
1119 that the archaeal KsgA-dependent methylations of the 16S rRNA are completed at a late stage of
1120 the small ribosomal subunit biogenesis in both *H. volcanii* and *P. furiosus*, and may predominantly
1121 occur after linearization of the circular-pre-16S rRNA. In contrast, helix 45 N⁴-cytidine acetylation,
1122 which is absent in *H. volcanii*, appears to be added at the circular-pre-16S rRNA stage, prior to
1123 completion of the KsgA-dependent modifications in *P. furiosus* (Fig. 7). These results are in good
1124 agreement with previous studies done in eukaryotes and bacteria^{104–106,108–111,141}. Moreover,
1125 expanding our sample-compare approach also suggests an increased amount of rRNA
1126 modifications in the hyperthermophile *P. furiosus*, and a decrease amount of predicted rRNA
1127 modifications in halophile *H. volcanii* in comparison to *E. coli*. These differential modification
1128 patterns across archaea are in good agreement with previous studies and may reflect adaptation
1129 to the environmental conditions that these extremophilic archaea encounter^{58,112,113}. Recently, it
1130 has been shown that *P. abyssi* 16S rRNA is heavily acetylated at CCG motifs⁵⁹. Our analysis suggests
1131 that N⁴-acetylcytidine modifications (i) increases the rate of basecalling errors (e.g. C>T) at the
1132 expected modified residue, (ii) are distributed across the 16S and 23S rRNA sequences in *P.*
1133 *furiosus*, and (iii) are successively added during rRNA maturation to reach “completeness” in the
1134 mature rRNAs. Future studies will be necessary to decipher, how widespread this type of
1135 modification is among archaea, and to evaluate their contribution for ribosomal subunit biogenesis
1136 and function in the cellular context.

1137 Whereas ONT may facilitate RNA modification analysis in general, the exact chemical nature of
1138 these modifications can not be unveiled without prior knowledge and remain a challenging task

1139 which greatly benefits of the use of unmodified/hypo-modified references (in agreement with
1140 recent studies^{16,138}). To facilitate high-throughput identification of RNA (DNA) modifications,
1141 future studies will required to develop and train algorithms improving the *de novo* identification
1142 confidence of diverse RNA/DNA modifications.

1143

1144 **Benefits and limitations of Nanopore-based native RNA sequencing**

1145 Taken together, a key advantage of the native RNA-seq approach is that multiple features can be
1146 addressed at once distinguishing the technique from the Illumina sequencing technology or
1147 biochemical assays. ONT sequencing does not require large scale equipment and is a fast method.
1148 Moreover, the method does not necessitate a reverse transcription step or PCR amplification
1149 thereby avoiding biases introduced by these enzymes. Due to the limitations of the sequencing
1150 read analysis platform, ONT sequencing does not accurately detect small RNAs yet. Additional
1151 limitations of the native RNA-seq technique are currently (i) the high amount of input RNA
1152 required (2-5 µg) to reach good coverage of the transcriptome without rRNA depletion, (ii) the
1153 need for a enzymatic poly-adenylation step of non polyA+ RNA, (iii) the 3' bias during RNA
1154 sequencing (iv) limited throughput and (v) limited possibilities for multiplexing. Although ONT
1155 sequencing has a comparably low sequencing accuracy, this did not pose a limitation for our
1156 analysis. Due to the extraordinary read length and the sensitivity to base modifications, ONT-based
1157 native RNA-seq can provide valuable insights into (r)RNA processing, (r)RNA modification
1158 patterns and the transcription of large operons. Strikingly, ONT-based sequencing is a *bona fide*
1159 single-molecule method and hence molecular heterogeneity in the transcriptome can be analysed
1160 so that even minor RNA populations can be detected that are inevitably lost in ensemble
1161 sequencing approaches.

1162

1163

1164 **Data availability**

1165 Raw sequencing data sets (gzipped raw FAST5 files) will be deposited in the Sequence Read
1166 Archive (SRA) and will be available under project accession number PRJNA632538.

1167

1168 **Code availability**

1169 A detailed documentation and code of all essential analysis steps (used tools and custom Rscripts)
1170 are available from https://github.com/felixgrunberger/Native_RNAseq_Microbes.

1171

1172 **Author contributions**

1173 F.G. established the nanopore workflow and performed all the bioinformatic analysis. F.G., R.K.,
1174 M.J., R.R. and A.B. performed RNA extractions. M.F. helped to optimize the RNA treatment protocol.
1175 F.G. carried out library preparations and performed sequencing. F.G., R.K., M.J. carried out *H.*
1176 *volcanii* wildtype/ $\Delta ksgA$ library preparations and sequencing. M.F. and R.R. performed
1177 transcription assays. R.K. and S.F.-C. generated the KsgA deletion strain. R.K. performed primer
1178 extension analysis. F.G., S.F.-C. and D.G. designed the study, analysed and interpreted the data, and
1179 wrote the manuscript with the input of all authors. J.S., W.H., S.F.-C. and D.G. supervised the
1180 experiments. S.F.-C. and D.G. initiated and supervised the project.

1181

1182 **Acknowledgements**

1183 We gratefully acknowledge financial support by the Deutsche Forschungsgemeinschaft within the
1184 collaborative research center framework (CRC/SFB960) "RNP biogenesis: assembly of ribosomes
1185 and non-ribosomal RNPs and control of their function" [SFB960-TP7 to D.G.] [SFB960-TP-B13 to
1186 S.F.-C.]. The work was also supported by the DFG through grant So264/21 to J.S.

1187

1188

1189 References

- 1190 1. Levy, S. E. & Myers, R. M. Advancements in Next-Generation Sequencing. *Annual review of genomics*
1191 *and human genetics* **17**, 95–115; 10.1146/annurev-genom-083115-022413 (2016).
- 1192 2. Escobar-Zepeda, A., Vera-Ponce de León, A. & Sanchez-Flores, A. The Road to Metagenomics: From
1193 Microbiology to DNA Sequencing Technologies and Bioinformatics. *Frontiers in Genetics* **6**, 348;
1194 10.3389/fgene.2015.00348 (2015).
- 1195 3. Wang, Z., Gerstein, M. & Snyder, M. RNA-Seq: a revolutionary tool for transcriptomics. *Nature*
1196 *reviews. Genetics* **10**, 57–63; 10.1038/nrg2484 (2009).
- 1197 4. Hör, J., Gorski, S. A. & Vogel, J. Bacterial RNA Biology on a Genome Scale. *Molecular cell* **70**, 785–
1198 799; 10.1016/j.molcel.2017.12.023 (2018).
- 1199 5. Croucher, N. J. & Thomson, N. R. Studying bacterial transcriptomes using RNA-seq. *Current opinion*
1200 *in microbiology* **13**, 619–624; 10.1016/j.mib.2010.09.009 (2010).
- 1201 6. Nowrousian, M. Next-generation sequencing techniques for eukaryotic microorganisms:
1202 sequencing-based solutions to biological problems. *Eukaryotic cell* **9**, 1300–1310;
1203 10.1128/EC.00123-10 (2010).
- 1204 7. Saliba, A.-E., C Santos, S. & Vogel, J. New RNA-seq approaches for the study of bacterial pathogens.
1205 *Current opinion in microbiology* **35**, 78–87; 10.1016/j.mib.2017.01.001 (2017).
- 1206 8. Stark, R., Grzelak, M. & Hadfield, J. RNA sequencing: the teenage years. *Nature Reviews Genetics*;
1207 10.1038/s41576-019-0150-2 (2019).
- 1208 9. Byrne, A., Cole, C., Volden, R. & Vollmers, C. Realizing the potential of full-length transcriptome
1209 sequencing. *Philosophical transactions of the Royal Society of London. Series B, Biological sciences*
1210 **374**, 20190097; 10.1098/rstb.2019.0097 (2019).
- 1211 10. Tilgner, H. *et al.* Comprehensive transcriptome analysis using synthetic long-read sequencing reveals
1212 molecular co-association of distant splicing events. *Nature Biotechnology* **33**, 736–742;
1213 10.1038/nbt.3242 (2015).
- 1214 11. Mikheyev, A. S. & Tin, M. M. Y. A first look at the Oxford Nanopore MinION sequencer. *Molecular*
1215 *ecology resources* **14**, 1097–1102; 10.1111/1755-0998.12324 (2014).
- 1216 12. Eid, J. *et al.* Real-time DNA sequencing from single polymerase molecules. *Science (New York, N.Y.)*
1217 **323**, 133–138; 10.1126/science.1162986 (2009).
- 1218 13. Sonesson, C. *et al.* A comprehensive examination of Nanopore native RNA sequencing for
1219 characterization of complex transcriptomes. *Nature Communications* **10**, 1–14; 10.1038/s41467-
1220 019-11272-z (2019).
- 1221 14. Vilfan, I. D. *et al.* Analysis of RNA base modification and structural rearrangement by single-molecule
1222 real-time detection of reverse transcription. *Journal of nanobiotechnology* **11**, 8; 10.1186/1477-
1223 3155-11-8 (2013).
- 1224 15. Liu, H. *et al.* Accurate detection of m6A RNA modifications in native RNA sequences. *Nature*
1225 *Communications*, 1–9; 10.1101/525741 (2019).
- 1226 16. Smith, A. M., Jain, M., Mulrone, L., Garalde, D. R. & Akesson, M. Reading canonical and modified
1227 nucleobases in 16S ribosomal RNA using nanopore native RNA sequencing. *PLOS ONE* **14**, 1–15;
1228 10.1371/journal.pone.0216709 (2019).
- 1229 17. Workman, R. E. *et al.* Nanopore native RNA sequencing of a human poly(A) transcriptome. *Nature*
1230 *Methods* **16**, 1297–1305; 10.1038/s41592-019-0617-2 (2019).
- 1231 18. Boldogkői, Z., Moldován, N., Balázs, Z., Snyder, M. & Tombácz, D. Long-Read Sequencing – A
1232 Powerful Tool in Viral Transcriptome Research. *Trends in Microbiology* **27**, 578–592;
1233 10.1016/j.tim.2019.01.010 (2019).
- 1234 19. Keller, M. W. *et al.* Direct RNA Sequencing of the Coding Complete Influenza A Virus Genome.
1235 *Scientific Reports* **8**, 1–8; 10.1038/s41598-018-32615-8 (2018).
- 1236 20. Viehweger, A. *et al.* Direct RNA nanopore sequencing of full-length coron-avirus genomes provides
1237 novel insights into structural variants and enables modification analysis. *bioRxiv*, 483693;
1238 10.1101/483693 (2019).
- 1239 21. Viehweger A, Krautwurst S, Lamkiewicz K, Madhugiri R, Ziebuhr J, Hölzer M, Marz M. Nanopore
1240 direct RNA sequencing reveals modification in full-length coronavirus genomes. *bioRxiv Genomics*,
1241 1–15; 10.1101/483693 (2018).
- 1242 22. Taiaroa, G. *et al.* *Direct RNA sequencing and early evolution of SARS-CoV-2* (2020).

- 1243 23. Tombácz, D. *et al.* Multiple Long-Read Sequencing Survey of Herpes Simplex Virus Dynamic
1244 Transcriptome. *Frontiers in Genetics* **10**, 834; 10.3389/fgene.2019.00834 (2019).
- 1245 24. Zhao, L. *et al.* Analysis of Transcriptome and Epitranscriptome in Plants Using PacBio Iso-Seq and
1246 Nanopore-Based Direct RNA Sequencing. *Frontiers in Genetics* **10**, 253; 10.3389/fgene.2019.00253
1247 (2019).
- 1248 25. Bayega, A. *et al.* *Transcriptome landscape of the developing olive fruit fly embryo delineated by*
1249 *Oxford Nanopore long-read RNA-Seq* (2018).
- 1250 26. Byrne, A. *et al.* Nanopore long-read RNAseq reveals widespread transcriptional variation among the
1251 surface receptors of individual B cells. *Nature Communications* **8**; 10.1038/ncomms16027 (2017).
- 1252 27. Rahimi, K., Venø, M. T., Dupont, D. M. & Kjems, J. *Nanopore sequencing of full-length circRNAs in*
1253 *human and mouse brains reveals circRNA-specific exon usage and intron retention* (2019).
- 1254 28. Dar, D. & Sorek, R. High-resolution RNA 3-ends mapping of bacterial Rho-dependent transcripts.
1255 *Nucleic Acids Research* **46**, 6797–6805; 10.1093/nar/gky274 (2018).
- 1256 29. Babski, J. *et al.* Genome-wide identification of transcriptional start sites in the haloarchaeon
1257 *Haloferax volcanii* based on differential RNA-Seq (dRNA-Seq). *BMC Genomics* **17**, 1–19;
1258 10.1186/s12864-016-2920-y (2016).
- 1259 30. Laass, S. *et al.* Characterization of the transcriptome of *Haloferax volcanii* , grown under four
1260 different conditions , with mixed RNA-Seq. *PLOS ONE* **14**, 1–24; 10.1371/journal.pone.0215986
1261 (2019).
- 1262 31. Mao, X. *et al.* Revisiting operons: An analysis of the landscape of transcriptional units in *E. coli*. *BMC*
1263 *Bioinformatics*; 10.1186/s12859-015-0805-8 (2015).
- 1264 32. Thomason, M. K. *et al.* Global transcriptional start site mapping using differential RNA sequencing
1265 reveals novel antisense RNAs in *Escherichia coli*. *Journal of Bacteriology* **197**, 18–28;
1266 10.1128/JB.02096-14 (2015).
- 1267 33. Grünberger, F. *et al.* Next Generation DNA-Seq and Differential RNA-Seq Allow Re-annotation of the
1268 *Pyrococcus furiosus* DSM 3638 Genome and Provide Insights Into Archaeal Antisense Transcription.
1269 *Frontiers in Microbiology*; 10.3389/fmicb.2019.01603 (2019).
- 1270 34. Stetter, K. O., König, H. & Stackebrandt, E. *Pyrodictium* gen. nov., a New Genus of Submarine Disc-
1271 Shaped Sulphur Reducing Archaeobacteria Growing Optimally at 105°C. *Systematic and Applied*
1272 *Microbiology*; 10.1016/S0723-2020(83)80011-3 (1983).
- 1273 35. Allers, T. & Mevarech, M. Archaeal genetics - the third way. *Nature Reviews Genetics* **6**, 58–73;
1274 10.1038/nrg1504 (2005).
- 1275 36. Knüppel, R. *et al.* Insights into the evolutionary conserved regulation of Rio ATPase activity. *Nucleic*
1276 *Acids Research* **46**, 1441–1456; 10.1093/nar/gkx1236 (2018).
- 1277 37. Chomczynski, P. & Sacchi, N. Single-step method of RNA isolation by acid guanidinium thiocyanate-
1278 phenol-chloroform extraction. *Analytical biochemistry* **162**, 156–159; 10.1006/abio.1987.9999
1279 (1987).
- 1280 38. Waege, I., Schmid, G., Thumann, S., Thomm, M. & Hausner, W. Shuttle vector-based transformation
1281 system for *Pyrococcus furiosus*. *Applied and environmental microbiology* **76**, 3308–3313;
1282 10.1128/AEM.01951-09 (2010).
- 1283 39. Hausner, W., Wettach, J., Hethke, C. & Thomm, M. Two transcription factors related with the
1284 eucaryal transcription factors TATA-binding protein and transcription factor IIB direct promoter
1285 recognition by an archaeal RNA polymerase. *The Journal of biological chemistry* **271**, 30144–30148;
1286 10.1074/jbc.271.47.30144 (1996).
- 1287 40. Kostrewa, D. *et al.* RNA polymerase II-TFIIB structure and mechanism of transcription initiation.
1288 *Nature* **462**, 323–330; 10.1038/nature08548 (2009).
- 1289 41. Spitalny, P. & Thomm, M. A polymerase III-like reinitiation mechanism is operating in regulation of
1290 histone expression in archaea. *Molecular microbiology* **67**, 958–970; 10.1111/j.1365-
1291 2958.2007.06084.x (2008).
- 1292 42. Dexl, S. *et al.* Displacement of the transcription factor B reader domain during transcription initiation.
1293 *Nucleic Acids Research* **46**, 10066–10081; 10.1093/nar/gky699 (2018).
- 1294 43. Ochs, S. M. *et al.* Activation of archaeal transcription mediated by recruitment of transcription factor
1295 B. *The Journal of biological chemistry* **287**, 18863–18871; 10.1074/jbc.M112.365742 (2012).
- 1296 44. Yan, B., Boitano, M., Clark, T. A. & Ettwiller, L. SMRT-Cappable-seq reveals complex operon variants
1297 in bacteria. *Nature Communications*; 10.1038/s41467-018-05997-6 (2018).

- 1298 45. Weirather, J. L. *et al.* Comprehensive comparison of Pacific Biosciences and Oxford Nanopore
1299 Technologies and their applications to transcriptome analysis. *F1000Research* **6**, 100;
1300 10.12688/f1000research.10571.2 (2017).
- 1301 46. Riley, M. *et al.* Escherichia coli K-12: a cooperatively developed annotation snapshot--2005. *Nucleic*
1302 *Acids Research* **34**, 1–9; 10.1093/nar/gkj405 (2006).
- 1303 47. Hartman, A. L. *et al.* The complete genome sequence of Haloferax volcanii DS2, a model archaeon.
1304 *PLOS ONE* **5**, e9605; 10.1371/journal.pone.0009605 (2010).
- 1305 48. Li, H. Minimap2: Pairwise alignment for nucleotide sequences. *Bioinformatics*;
1306 10.1093/bioinformatics/bty191 (2018).
- 1307 49. Li, H. *et al.* The Sequence Alignment/Map format and SAMtools. *Bioinformatics* **25**, 2078–2079;
1308 10.1093/bioinformatics/btp352 (2009).
- 1309 50. Liao, Y., Smyth, G. K. & Shi, W. The R package Rsubread is easier, faster, cheaper and better for
1310 alignment and quantification of RNA sequencing reads. *Nucleic Acids Research*; 10.1093/nar/gkz114
1311 (2019).
- 1312 51. Love, M. I., Huber, W. & Anders, S. Moderated estimation of fold change and dispersion for RNA-seq
1313 data with DESeq2. *Genome Biology* **15**, 550; 10.1186/s13059-014-0550-8 (2014).
- 1314 52. Loman, N. J., Quick, J. & Simpson, J. T. A complete bacterial genome assembled de novo using only
1315 nanopore sequencing data. *Nature Methods* **12**, 733–735; 10.1038/nmeth.3444 (2015).
- 1316 53. Bailey, T. L. *et al.* MEME SUITE: tools for motif discovery and searching. *Nucleic Acids Research* **37**,
1317 W202–8; 10.1093/nar/gkp335 (2009).
- 1318 54. Dar, D., Prasse, D., Schmitz, R. A. & Sorek, R. Widespread formation of alternative 3' UTR isoforms
1319 via transcription termination in archaea. *Nature Microbiology* **1**, 16143;
1320 10.1038/nmicrobiol.2016.143 (2016).
- 1321 55. Lorenz, R. *et al.* ViennaRNA Package 2.0. *Algorithms for molecular biology : AMB* **6**, 26;
1322 10.1186/1748-7188-6-26 (2011).
- 1323 56. Berkemer, S. J. *et al.* Identification of RNA 3' ends and termination sites in Haloferax volcanii. *RNA*
1324 *Biology*, 1–14; 10.1080/15476286.2020.1723328 (2020).
- 1325 57. Stoiber, M. *et al.* De novo Identification of DNA Modifications Enabled by Genome-Guided Nanopore
1326 Signal Processing (2016).
- 1327 58. Grosjean, H., Gaspin, C., Marck, C., Decatur, W. A. & Crécy-Lagard, V. de. RNomics and Modomics in
1328 the halophilic archaea Haloferax volcanii: Identification of RNA modification genes. *BMC Genomics*
1329 **9**, 1–26; 10.1186/1471-2164-9-470 (2008).
- 1330 59. Coureux, P.-D., Lazennec-Schurdevin, C., Bourcier, S., Mechulam, Y. & Schmitt, E. Cryo-EM study of
1331 an archaeal 30S initiation complex gives insights into evolution of translation initiation.
1332 *Communications biology* **3**, 58; 10.1038/s42003-020-0780-0 (2020).
- 1333 60. Mao, X. *et al.* DOOR 2.0: Presenting operons and their functions through dynamic and integrated
1334 views. *Nucleic Acids Research* **42**; 10.1093/nar/gkt1048 (2014).
- 1335 61. Bolger, A. M., Lohse, M. & Usadel, B. Trimmomatic: a flexible trimmer for Illumina sequence data.
1336 *Bioinformatics* **30**, 2114–2120; 10.1093/bioinformatics/btu170 (2014).
- 1337 62. Langmead, B. & Salzberg, S. L. Fast gapped-read alignment with Bowtie 2. *Nature Methods* **9**, 357–
1338 359; 10.1038/nmeth.1923 (2012).
- 1339 63. Bohlin, J., Eldholm, V., Pettersson, J. H. O., Brynildsrud, O. & Snipen, L. The nucleotide composition
1340 of microbial genomes indicates differential patterns of selection on core and accessory genomes.
1341 *BMC Genomics* **18**, 151; 10.1186/s12864-017-3543-7 (2017).
- 1342 64. Wick, R. R., Judd, L. M. & Holt, K. E. Performance of neural network basecalling tools for Oxford
1343 Nanopore sequencing. *Genome Biology* **20**, 1–10; 10.1186/s13059-019-1727-y (2019).
- 1344 65. Garalde, D. R. *et al.* Highly parallel direct RNA sequencing on an array of nanopores. *Nature Methods*
1345 **15**, 201–206; 10.1038/nmeth.4577 (2018).
- 1346 66. Workman, R. E. *et al.* Nanopore native RNA sequencing of a human poly(A) transcriptome. *bioRxiv*;
1347 10.1101/459529 (2018).
- 1348 67. Parker, M. T. *et al.* Nanopore direct RNA sequencing maps an Arabidopsis N6 methyladenosine
1349 epitranscriptome. *bioRxiv*; 10.1101/706002 (2019).
- 1350 68. Ju, X., Li, D. & Liu, S. Full-length RNA profiling reveals pervasive bidirectional transcription
1351 terminators in bacteria. *Nature Microbiology*; 10.1038/s41564-019-0500-z (2019).
- 1352 69. Mitra, P., Ghosh, G., Hafeezunnisa, M. & Sen, R. Rho Protein: Roles and Mechanisms. *Annual review*
1353 *of microbiology* **71**, 687–709; 10.1146/annurev-micro-030117-020432 (2017).

- 1354 70. Sanders, T. J. *et al.* FttA is a CPSF73 homologue that terminates transcription in Archaea. *Nature*
1355 *Microbiology*; 10.1038/s41564-020-0667-3 (2020).
- 1356 71. Ray-Soni, A., Bellecourt, M. J. & Landick, R. Mechanisms of Bacterial Transcription Termination: All
1357 Good Things Must End. *Annual review of biochemistry* **85**, 319–347; 10.1146/annurev-biochem-
1358 060815-014844 (2016).
- 1359 72. Santangelo, T. J., Cubonová, L.'u., Skinner, K. M. & Reeve, J. N. Archaeal intrinsic transcription
1360 termination in vivo. *Journal of Bacteriology* **191**, 7102–7108; 10.1128/JB.00982-09 (2009).
- 1361 73. Berkemer, S. J. *et al.* Identification of RNA 3' ends and termination sites in *Haloferax volcanii* (2019).
- 1362 74. Liang, W., Rudd, K. E. & Deutscher, M. P. A role for REP sequences in regulating translation. *Molecular*
1363 *cell* **58**, 431–439; 10.1016/j.molcel.2015.03.019 (2015).
- 1364 75. Khemici, V. & Carpousis, A. J. The RNA degradosome and poly(A) polymerase of *Escherichia coli* are
1365 required in vivo for the degradation of small mRNA decay intermediates containing REP-stabilizers.
1366 *Molecular microbiology* **51**, 777–790; 10.1046/j.1365-2958.2003.03862.x (2004).
- 1367 76. Smith, A. M. *et al.* Reading canonical and modified nucleotides in 16S ribosomal RNA using nanopore
1368 direct RNA sequencing. *bioRxiv*; 10.1101/132274 (2017).
- 1369 77. Wongsurawat, T. *et al.* Rapid sequencing of multiple RNA viruses in their native form. *Frontiers in*
1370 *Microbiology* **10**, 1–8; 10.3389/fmicb.2019.00260 (2019).
- 1371 78. Näther-Schindler, D. J., Schopf, S., Bellack, A., Rachel, R. & Wirth, R. *Pyrococcus furiosus* flagella:
1372 biochemical and transcriptional analyses identify the newly detected flaBO gene to encode the major
1373 flagellin. *Frontiers in Microbiology* **5**, 695; 10.3389/fmicb.2014.00695 (2014).
- 1374 79. Lioliou, E. *et al.* Global regulatory functions of the *Staphylococcus aureus* endoribonuclease III in
1375 gene expression. *PLoS Genetics* **8**, e1002782; 10.1371/journal.pgen.1002782 (2012).
- 1376 80. Smith, B. A., Gupta, N., Denny, K. & Culver, G. M. Characterization of 16S rRNA Processing with Pre-
1377 30S Subunit Assembly Intermediates from *E. coli*. *Journal of Molecular Biology*;
1378 10.1016/j.jmb.2018.04.009 (2018).
- 1379 81. Shajani, Z., Sykes, M. T. & Williamson, J. R. Assembly of bacterial ribosomes. *Annual review of*
1380 *biochemistry* **80**, 501–526; 10.1146/annurev-biochem-062608-160432 (2011).
- 1381 82. Bechhofer, D. H. & Deutscher, M. P. Bacterial ribonucleases and their roles in RNA metabolism.
1382 *Critical reviews in biochemistry and molecular biology* **54**, 242–300;
1383 10.1080/10409238.2019.1651816 (2019).
- 1384 83. Klappenbach, J. A., Saxman, P. R., Cole, J. R. & Schmidt, T. M. rrndb: the Ribosomal RNA Operon Copy
1385 Number Database. *Nucleic Acids Research* **29**, 181–184; 10.1093/nar/29.1.181 (2001).
- 1386 84. Maeda, M., Shimada, T., Ishihama, A. & Semsey, S. Strength and Regulation of Seven rRNA Promoters
1387 in *Escherichia coli*. *PLOS ONE* **10**, e0144697; 10.1371/journal.pone.0144697 (2015).
- 1388 85. Jain, C. RNase AM, a 5' to 3' exonuclease, matures the 5' end of all three ribosomal RNAs in *E. coli*.
1389 *Nucleic Acids Research*; 10.1093/nar/gkaa260 (2020).
- 1390 86. Hofmann, S. & Miller, O. L. Visualization of ribosomal ribonucleic acid synthesis in a ribonuclease III-
1391 Deficient strain of *Escherichia coli*. *Journal of Bacteriology* **132**, 718–722 (1977).
- 1392 87. Jacob, A. I., Köhrer, C., Davies, B. W., RajBhandary, U. L. & Walker, G. C. Conserved bacterial RNase
1393 YbeY plays key roles in 70S ribosome quality control and 16S rRNA maturation. *Molecular cell* **49**,
1394 427–438; 10.1016/j.molcel.2012.11.025 (2013).
- 1395 88. Yip, W. S. V., Vincent, N. G. & Baserga, S. J. Ribonucleoproteins in archaeal pre-rRNA processing and
1396 modification. *Archaea (Vancouver, B.C.)* **2013**, 614735; 10.1155/2013/614735 (2013).
- 1397 89. Ferreira-Cerca, S. in *RNA Metabolism and Gene Expression in Archaea*, edited by B. Clouet-d'Orval
1398 (Springer International Publishing, Cham, 2017), pp. 129–158.
- 1399 90. Henras, A. K., Plisson-Chastang, C., O'Donohue, M.-F., Chakraborty, A. & Gleizes, P.-E. An overview
1400 of pre-ribosomal RNA processing in eukaryotes. *Wiley interdisciplinary reviews. RNA* **6**, 225–242;
1401 10.1002/wrna.1269 (2015).
- 1402 91. Clouet-D'Orval, B. *et al.* Insights into RNA-processing pathways and associated RNA-degrading
1403 enzymes in Archaea. *FEMS Microbiology Reviews* **42**, 579–613; 10.1093/femsre/fuy016 (2018).
- 1404 92. Tang, T. H. *et al.* RNomics in Archaea reveals a further link between splicing of archaeal introns and
1405 rRNA processing. *Nucleic Acids Research* **30**, 921–930; 10.1093/nar/30.4.921 (2002).
- 1406 93. Russell, A. G., Ebhardt, H. & Dennis, P. P. Substrate requirements for a novel archaeal endonuclease
1407 that cleaves within the 5' external transcribed spacer of *Sulfolobus acidocaldarius* precursor rRNA.
1408 *Genetics* **152**, 1373–1385 (1999).
- 1409 94. Danan, M., Schwartz, S., Edelheit, S. & Sorek, R. Transcriptome-wide discovery of circular RNAs in
1410 Archaea. *Nucleic Acids Research* **40**, 3131–3142; 10.1093/nar/gkr1009 (2012).

- 1411 95. Jüttner, M. *et al.* A versatile cis-acting element reporter system to study the function, maturation
1412 and stability of ribosomal RNA mutants in archaea. *Nucleic Acids Research*; 10.1093/nar/gkz1156
1413 (2019).
- 1414 96. Qi, L., Li, J., Jia, J., Yue, L. & Dong, X. Comprehensive analysis of the pre-ribosomal RNA maturation
1415 pathway in a methanoarchaeon exposes the conserved circularization and linearization mode in
1416 archaea. *RNA Biology*; 10.1080/15476286.2020.1771946 (2020).
- 1417 97. Ferreira-Cerca, S. *RNA Metabolism and Gene Expression in Archaea - Chapter6 - Life and Death of*
1418 *Ribosomes in Archaea* (2017).
- 1419 98. Durovic, P. & Dennis, P. P. Separate pathways for excision and processing of 16S and 23S rRNA from
1420 the primary rRNA operon transcript from the hyperthermophilic archaeobacterium *Sulfolobus*
1421 *acidocaldarius*: similarities to eukaryotic rRNA processing. *Molecular microbiology* **13**, 229–242;
1422 10.1111/j.1365-2958.1994.tb00418.x (1994).
- 1423 99. Boccaletto, P. *et al.* MODOMICS: a database of RNA modification pathways. 2017 update. *Nucleic*
1424 *Acids Research* **46**, D303-D307; 10.1093/nar/gkx1030 (2018).
- 1425 100. Wongsurawat, T. *et al.* Decoding the Epitranscriptional Landscape from Native RNA Sequences.
1426 *bioRxiv* **17**, 487819; 10.1101/487819 (2018).
- 1427 101. Rand, A. C. *et al.* Mapping DNA methylation with high-throughput nanopore sequencing. *Nature*
1428 *Methods* **14**, 411–413; 10.1038/nmeth.4189 (2017).
- 1429 102. O'Farrell, H. C., Pulicherla, N., Desai, P. M. & Rife, J. P. Recognition of a complex substrate by
1430 the KsgA/Dim1 family of enzymes has been conserved throughout evolution. *RNA (New York, N.Y.)*
1431 **12**, 725–733; 10.1261/rna.2310406 (2006).
- 1432 103. Rang, F. J., Kloosterman, W. P. & Ridder, J. de. From squiggle to basepair: Computational
1433 approaches for improving nanopore sequencing read accuracy. *Genome Biology* **19**, 1–11;
1434 10.1186/s13059-018-1462-9 (2018).
- 1435 104. Strunk, B. S. *et al.* Ribosome assembly factors prevent premature translation initiation by 40S
1436 assembly intermediates. *Science (New York, N.Y.)* **333**, 1449–1453; 10.1126/science.1208245
1437 (2011).
- 1438 105. Xu, Z., O'Farrell, H. C., Rife, J. P. & Culver, G. M. A conserved rRNA methyltransferase regulates
1439 ribosome biogenesis. *Nature structural & molecular biology* **15**, 534–536; 10.1038/nsmb.1408
1440 (2008).
- 1441 106. Lafontaine, D. L., Preiss, T. & Tollervey, D. Yeast 18S rRNA dimethylase Dim1p: a quality control
1442 mechanism in ribosome synthesis? *Molecular and cellular biology* **18**, 2360–2370;
1443 10.1128/mcb.18.4.2360 (1998).
- 1444 107. Iost, I., Chabas, S. & Darfeuille, F. Maturation of atypical ribosomal RNA precursors in
1445 *Helicobacter pylori*. *Nucleic Acids Research* **47**, 5906–5921; 10.1093/nar/gkz258 (2019).
- 1446 108. Ito, S. *et al.* A single acetylation of 18 S rRNA is essential for biogenesis of the small ribosomal
1447 subunit in *Saccharomyces cerevisiae*. *The Journal of biological chemistry* **289**, 26201–26212;
1448 10.1074/jbc.M114.593996 (2014).
- 1449 109. Sharma, S. *et al.* Yeast Kre33 and human NAT10 are conserved 18S rRNA cytosine
1450 acetyltransferases that modify tRNAs assisted by the adaptor Tan1/THUMP1. *Nucleic Acids*
1451 *Research* **43**, 2242–2258; 10.1093/nar/gkv075 (2015).
- 1452 110. Sharma, S. *et al.* Specialized box C/D snoRNPs act as antisense guides to target RNA base
1453 acetylation. *PLoS Genetics* **13**, e1006804; 10.1371/journal.pgen.1006804 (2017).
- 1454 111. Sleiman, S. & Dragon, F. Recent Advances on the Structure and Function of RNA
1455 Acetyltransferase Kre33/NAT10. *Cells* **8**; 10.3390/cells8091035 (2019).
- 1456 112. Dennis, P. P., Tripp, V., Lui, L., Lowe, T. & Randau, L. C/D box sRNA-guided 2'-O-methylation
1457 patterns of archaeal rRNA molecules. *BMC Genomics*; 10.1186/s12864-015-1839-z (2015).
- 1458 113. Gomes-Filho, J. V. & Randau, L. RNA stabilization in hyperthermophilic archaea. *Annals of the*
1459 *New York Academy of Sciences* **1447**, 88–96; 10.1111/nyas.14060 (2019).
- 1460 114. Ebright, R. H., Werner, F. & Zhang, X. RNA Polymerase Reaches 60: Transcription Initiation,
1461 Elongation, Termination, and Regulation in Prokaryotes. *Journal of Molecular Biology* **431**, 3945–
1462 3946; 10.1016/j.jmb.2019.07.026 (2019).
- 1463 115. Babski, J. *et al.* Small regulatory RNAs in Archaea. *RNA Biology* **11**, 484–493; 10.4161/rna.28452
1464 (2014).
- 1465 116. Oliva, G., Sahr, T. & Buchrieser, C. Small RNAs, 5' UTR elements and RNA-binding proteins in
1466 intracellular bacteria: impact on metabolism and virulence. *FEMS Microbiology Reviews* **39**, 331–
1467 349; 10.1093/femsre/fuv022 (2015).

- 1468 117. Ren, G.-X., Guo, X.-P. & Sun, Y.-C. Regulatory 3' Untranslated Regions of Bacterial mRNAs.
1469 *Frontiers in Microbiology* **8**, 1276; 10.3389/fmicb.2017.01276 (2017).
- 1470 118. Hirtreiter, A. *et al.* Spt4/5 stimulates transcription elongation through the RNA polymerase
1471 clamp coiled-coil motif. *Nucleic Acids Research* **38**, 4040–4051; 10.1093/nar/gkq135 (2010).
- 1472 119. Hirtreiter, A., Grohmann, D. & Werner, F. Molecular mechanisms of RNA polymerase--the F/E
1473 (RPB4/7) complex is required for high processivity in vitro. *Nucleic Acids Research* **38**, 585–596;
1474 10.1093/nar/gkp928 (2010).
- 1475 120. Yue, L. *et al.* *aCPSF1 controlled archaeal transcription termination: a prototypical eukaryotic*
1476 *model* (2019).
- 1477 121. French, S. L., Santangelo, T. J., Beyer, A. L. & Reeve, J. N. Transcription and translation are
1478 coupled in Archaea. *Molecular biology and evolution* **24**, 893–895; 10.1093/molbev/msm007 (2007).
- 1479 122. Webster, M. W. *et al.* *Structural basis of transcription-translation coupling and collision in*
1480 *bacteria* (2020).
- 1481 123. O'Reilly, F. J. *et al.* *In-cell architecture of an actively transcribing-translating expressome* (2020).
- 1482 124. Vogel, U. & Jensen, K. F. The RNA chain elongation rate in Escherichia coli depends on the
1483 growth rate. *Journal of Bacteriology* **176**, 2807–2813; 10.1128/jb.176.10.2807-2813.1994 (1994).
- 1484 125. Proshkin, S., Rahmouni, A. R., Mironov, A. & Nudler, E. Cooperation between translating
1485 ribosomes and RNA polymerase in transcription elongation. *Science (New York, N.Y.)* **328**, 504–508;
1486 10.1126/science.1184939 (2010).
- 1487 126. Stevenson-Jones, F., Woodgate, J., Castro-Roa, D. & Zenkin, N. Ribosome reactivates
1488 transcription by physically pushing RNA polymerase out of transcription arrest. *Proceedings of the*
1489 *National Academy of Sciences of the United States of America* **117**, 8462–8467;
1490 10.1073/pnas.1919985117 (2020).
- 1491 127. Albers, S.-V. & Jarrell, K. F. The archaeellum: how Archaea swim. *Frontiers in Microbiology* **6**, 23;
1492 10.3389/fmicb.2015.00023 (2015).
- 1493 128. Daum, B. *et al.* Structure and in situ organisation of the Pyrococcus furiosus archaeellum
1494 machinery. *eLife* **6**; 10.7554/eLife.27470 (2017).
- 1495 129. Deutscher, M. P. Twenty years of bacterial RNases and RNA processing: how we've matured.
1496 *RNA (New York, N.Y.)* **21**, 597–600; 10.1261/rna.049692.115 (2015).
- 1497 130. Venema, J. & Tollervey, D. Processing of pre-ribosomal RNA in Saccharomyces cerevisiae. *Yeast*
1498 *(Chichester, England)* **11**, 1629–1650; 10.1002/yea.320111607 (1995).
- 1499 131. Nikolaev, N., Silengo, L. & Schlessinger, D. Synthesis of a large precursor to ribosomal RNA in a
1500 mutant of Escherichia coli. *Proceedings of the National Academy of Sciences of the United States of*
1501 *America* **70**, 3361–3365; 10.1073/pnas.70.12.3361 (1973).
- 1502 132. LITTLEFIELD, J. W. & DUNN, D. B. Natural occurrence of thymine and three methylated adenine
1503 bases in several ribonucleic acids. *Nature* **181**, 254–255; 10.1038/181254a0 (1958).
- 1504 133. SMITH, J. D. & DUNN, D. B. The occurrence of methylated guanines in ribonucleic acids from
1505 several sources. *The Biochemical journal* **72**, 294–301; 10.1042/bj0720294 (1959).
- 1506 134. Li, S. & Mason, C. E. The pivotal regulatory landscape of RNA modifications. *Annual review of*
1507 *genomics and human genetics* **15**, 127–150; 10.1146/annurev-genom-090413-025405 (2014).
- 1508 135. Schwartz, S. & Motorin, Y. Next-generation sequencing technologies for detection of modified
1509 nucleotides in RNAs. *RNA Biology* **14**, 1124–1137; 10.1080/15476286.2016.1251543 (2017).
- 1510 136. Sas-Chen, A. & Schwartz, S. Misincorporation signatures for detecting modifications in mRNA:
1511 Not as simple as it sounds. *Methods (San Diego, Calif.)* **156**, 53–59; 10.1016/j.ymeth.2018.10.011
1512 (2019).
- 1513 137. Lorenz, D. A., Sathe, S., Einstein, J. M. & Yeo, G. W. Direct RNA sequencing enables m6A
1514 detection in endogenous transcript isoforms at base specific resolution. *RNA (New York, N.Y.)*;
1515 10.1261/rna.072785.119 (2019).
- 1516 138. Leger, A. *et al.* *RNA modifications detection by comparative Nanopore direct RNA sequencing*
1517 (2019).
- 1518 139. Ebersberger, I. *et al.* The evolution of the ribosome biogenesis pathway from a yeast
1519 perspective. *Nucleic Acids Research* **42**, 1509–1523; 10.1093/nar/gkt1137 (2014).
- 1520 140. Grosjean, H., Gaspin, C., Marck, C., Decatur, W. A. & Crécy-Lagard, V. de. RNomics and
1521 Modomics in the halophilic archaea Haloferax volcanii: identification of RNA modification genes.
1522 *BMC Genomics* **9**, 470; 10.1186/1471-2164-9-470 (2008).

- 1523 141. Ito, S. *et al.* Human NAT10 is an ATP-dependent RNA acetyltransferase responsible for N4-
1524 acetylcytidine formation in 18 S ribosomal RNA (rRNA). *The Journal of biological chemistry* **289**,
1525 35724–35730; 10.1074/jbc.C114.602698 (2014).
1526 142. Yu, S.-H., Vogel, J. & Förstner, K. U. *ANNOgesic: A Swiss army knife for the RNA-Seq based*
1527 *annotation of bacterial/archaeal genomes* (2017).
1528